Accepted Manuscript

MFSD2A Promotes Endothelial Generation of Inflammation-resolving Lipid Mediators and Reduces Colitis in Mice

Federica Ungaro, Carlotta Tacconi, Luca Massimino, Paola Antonia Corsetto, Carmen Correale, Philippe Fonteyne, Andrea Piontini, Valeria Garzarelli, Francesca Calcaterra, Silvia Della Bella, Antonino Spinelli, Michele Carvello, Angela Maria Rizzo, Stefania Vetrano, Luciana Petti, Gionata Fiorino, Federica Furfaro, Domenico Mavilio, Krishna Rao Maddipati, Alberto Malesci, Laurent Peyrin-Biroulet, Silvia D'Alessio, Silvio Danese

PII: S0016-5085(17)35988-7
DOI: 10.1053/j.gastro.2017.07.048
Reference: YGAST 61348

To appear in: *Gastroenterology*
Accepted Date: 30 July 2017

Please cite this article as: Ungaro F, Tacconi C, Massimino L, Corsetto PA, Correale C, Fonteyne P, Piontini A, Garzarelli V, Calcaterra F, Della Bella S, Spinelli A, Carvello M, Rizzo AM, Vetrano S, Petti L, Fiorino G, Furfaro F, Mavilio D, Maddipati KR, Malesci A, Peyrin-Biroulet L, D'Alessio S, Danese S, MFSD2A Promotes Endothelial Generation of Inflammation-resolving Lipid Mediators and Reduces Colitis in Mice, *Gastroenterology* (2017), doi: 10.1053/j.gastro.2017.07.048.

MFSD2A Promotes Endothelial Generation of Inflammation-resolving Lipid Mediators and Reduces Colitis in Mice

Federica Ungaro[1,2], Carlotta Tacconi[3], Luca Massimino[4], Paola Antonia Corsetto[5], Carmen Correale[1], Philippe Fonteyne[1], Andrea Piontini[1,2], Valeria Garzarelli[1], Francesca Calcaterra[6,7], Silvia Della Bella[6,7], Antonino Spinelli[2,8], Michele Carvello[8], Angela Maria Rizzo[5], Stefania Vetrano[1,2], Luciana Petti[1,7], Gionata Fiorino[1], Federica Furfaro[1], Domenico Mavilio[6,7], Krishna Rao Maddipati[9], Alberto Malesci[7,10], Laurent Peyrin-Biroulet[11], Silvia D'Alessio[1,7,*] and Silvio Danese[1,2,*]

[1] IBD Center, Laboratory of Gastrointestinal Immunopathology, Humanitas Clinical and Research Center, Rozzano, Milan, Italy

[2] Department of Biomedical Sciences, Humanitas University, Rozzano, Milan, Italy

[3] Institute of Pharmaceutical Sciences, Pharmacogenomics, Swiss Federal Institute of Technology (ETH) Zurich, Switzerland

[4] School of medicine and surgery, University of Milan-Bicocca, Milan, Italy

[5] Department of Pharmacology and Biomolecular Science, University of Milan

[6] Laboratory of Clinical and Experimental Immunology, Humanitas Clinical and Research Center, Rozzano, Milan, Italy

[7] Department of Medical Biotechnologies and Translational Medicine, University of Milan, Italy

[8] Colon and Rectal Surgery Unit, Humanitas Clinical and Research Center, Rozzano, Milan, Italy

[9] Department of Pathology, Lipdomics Core Facility, Wayne State University, Detroit, USA

[10] Department of Gastroenterology, Humanitas Clinical and Research Center, Rozzano, Milan, Italy.

[11] Institut National de la Santé et de la Recherche Médicale U954 and Department of Gastroenterology, Nancy University Hospital, Lorraine University, France.

* These authors share co-senior authorship.

Grant Support

This study was supported by grants from the Broad Medical Research Program (510262) to S.D.; the Italian Ministry of Health (RBFR12VP3Q_002) to S.D. ; the Innovative Medicines Initiative (IMI) Joint Undertaking BTCure (115142) to S.D.; The work was conducted in the context, and with the support, of the Fondazione Humanitas per la Ricerca (Rozzano, Italy).

Abbreviations

Inflammatory Bowel Disease, IBD; Crohn's Disease, CD; Ulcerative Colitis, UC; Major Facilitator Superfamily Domain Containing 2A, MFSD2A; docosahexaenoic acid, DHA; circulating endothelial colony-forming cells, ECFCs; human intestinal microvascular endothelial cells, HIMECs; overexpressing, -OE; polyunsaturated fatty acids, PUFAs; cytochrome *P*-450, CYP450; Arachidonic Acid, AA; Dihomo-γ-linolenic Acid, DGLA; Linoleic Acid, LA; Eicosapentaenoic Acid, EPA; Linolenic Acid, LNA; Principal components analysis; PCA; Liquid Chromatography tandem mass spectrometry, LC-MS/MS; cyclooxygenases, COX; lipoxygenases, LOX; epoxydocosapentaenoic acids, EpDPEs; Plasmalemmal vesicle-1, PV1.

Corresponding authors

Silvio Danese, Humanitas Clinical and Research Center, Laboratory of Gastrointestinal Immunopathology, Via Manzoni 113, 20089 Rozzano (MI), Italy; TEL. +390282244771; FAX: +390282245101. Email: sdanese@hotmail.com.

Silvia D'Alessio, Humanitas Clinical and Research Center, Laboratory of Gastrointestinal Immunopathology, Via Manzoni 113, 20089 Rozzano (MI), Italy; TEL. +390282245146; FAX: +390282245101. Email: silvia.dalessio@humanitasresearch.it

Disclosure

The authors disclose no conflicts

Author Contributions

Conceptualization, F.U. and S.DA.; Methodology, F.U. and S.DA.; Formal Analysis, F.U. and L.M.; Investigation, F.U., S.DA., C.T., P.A.C., C.C., P.F., A.P., V.G., A.M.R., and K.R.M.

Resources, F.C., S.DB., A.S., M.C., G.F., F.F. and D.M.; Writing – Original Draft, S.DA. and F.U.; Writing – Review & Editing, C.T., C.C., P.A.C., A.M.R., S.V., L.P., K.R.M., A.M., L.PB. and S.D.; Visualization, F.U. and S.DA.; Supervision, S.DA.; Project Administration, S.DA.; Funding Acquisition, S.D.

Abstract:

Background & Aims: Alterations in signaling pathways that regulate resolution of inflammation (resolving pathways) contribute to pathogenesis of ulcerative colitis (UC). The resolution process is regulated by lipid mediators, such as those derived from the ω-3 docosahexaenoic acid (DHA), whose esterified form is transported by the major facilitator superfamily domain containing 2A (MFSD2A) through the endothelium of brain, retina, and placenta. We investigated if and how MFSD2A regulates lipid metabolism of gut endothelial cells to promote resolution of intestinal inflammation.

Methods: We performed lipidomic and functional analyses of MFSD2A in mucosal biopsies and primary human intestinal microvascular endothelial cells (HIMECs) isolated from surgical specimens from patients with active, resolving UC and healthy individuals without UC (controls). MFSD2A was knocked down in HIMECss with small hairpin RNAs or overexpressed from a lentiviral vector. Human circulating endothelial progenitor cells that overexpress MFSD2A were transferred to CD1 nude mice with dextran sodium sulfate-induced colitis, with or without oral administration of DHA.

Results: Colonic biopsies from patients with UC had reduced levels of inflammation-resolving DHA-derived epoxy metabolites compared to healthy colon tissues or tissues with resolution of inflammation. Production of these metabolites by HIMECs required MFSD2A, which is required for DHA retention and metabolism in the gut vasculature. In mice with colitis, transplanted endothelial progenitor cells that overexpressed MFSD2A not only localized to the inflamed mucosa but also restored the ability of the endothelium to resolve intestinal inflammation, compared to mice with colitis that did not receive MFSD2A-overexpressing endothelial progenitors

Conclusions: Levels of DHA-derived epoxides are lower in colon tissues from patients with UC than healthy and resolving mucosa. Production of these metabolites by gut endothelium requires MFSD2A; endothelial progenitor cells that overexpress MFSD2A reduce colitis in mice. This pathway might be induced to resolve intestinal inflammation in patients with colitis.

Key words

inflammatory bowel disease, IBD, gut vasculature, angiogenesis

Introduction

Ulcerative colitis (UC) is a long-term idiopathic inflammatory disorder affecting the colon and rectum, whose prevalence and incidence is rapidly increasing worldwide, and whose medical treatments have only been mildly successful[1]. For many years, dysregulations in inflammatory pathways have been considered as the basis of UC pathogenesis; nevertheless, the simple targeting of infiltrating immune cells and their products to control inflammation does not always lead to remission. New evidences indicate that a failure in resolving pathways might also contribute to the pathogenesis of this disease[2,3]. Indeed, only recently the resolution of inflammation has been conclusively recognized as an active process orchestrated by resolving lipid mediators, which dampen inflammation-sustaining events, such as angiogenesis, release of inflammatory cytokines, clearance of apoptotic cells and microorganisms[4,5]. Among these resolving molecules, those derived from essential ω-3-polyunsaturated fatty acids (PUFAs), have been shown to exert beneficial effects on a wide range of human inflammatory disorders, including UC[6]. In particular, epoxy metabolites of docosahexaenoic acid (DHA), generated by cytochrome *P*-450 (CYP450) enzymes, promote potent biological activities in the regulation of vascular, pulmonary, cardiac and intestinal functions[7,8].

The progression of chronic intestinal inflammation is not only orchestrated by immune cells, but also non-immune cells, and particularly by endothelial cells. In fact, UC patients are characterized by increased vascularization and excessive release of angiogenic factors[9]. The ability of endothelial cells to secrete anti-inflammatory mediators, which help to coordinate leukocyte trafficking and maintain barrier function, renders them crucial players in the resolution of inflammation[10]. Seminal studies have pointed out the pro-resolving beneficial effects of ω-3 DHA on endothelial cells under inflammatory conditions[8,11]. Although the endothelium plays a major role in resolution of inflammation, the exact mechanisms behind this process are still unknown, particularly in the gastrointestinal tract. The endothelial lysophosphatidylcholine transporter, namely the major facilitator superfamily domain

containing 2A (MFSD2A), has recently been shown to be essential for DHA uptake in the blood brain barrier, eye and placenta[12–14]. Here we elucidate a significant role for MFSD2A in the maintenance of the balance between inflammatory and resolving epoxy metabolites of DHA in intestinal microvasculature and how this could be used for the development of novel therapeutic strategies to treat UC.

Material and methods

Detailed protocols are provided in the Supplementary Material and Methods.

Results

Lipid signature of intestinal mucosa from patients with active UC highlights defects in DHA metabolite production

PUFAs are known to regulate the duration and magnitude of inflammation, with ω-6 fatty acids mostly as inflammatory and ω-3 fatty acids as resolving molecules[15]. In order to define the fatty acyl signature of patients with UC, endoscopic biopsies collected from the colon of actively inflamed, and resolving patients, including healthy tissues (**Supplementary Table 1** for patient characteristics), were characterized by liquid chromatography-tandem mass spectrometry (LC-MS/MS). Lipid mediators were classified on the basis of their precursors: ω-6 Arachidonic Acid (AA), Dihomo-γ-linolenic Acid (DGLA) and Linoleic Acid (LA), and the ω-3 DHA, Eicosapentaenoic Acid (EPA) and Linolenic Acid (LNA). Principal components analysis (PCA) performed on LC-MS/MS data output highlighted a distinct lipid signature of actively inflamed biopsies, while healthy tissues and tissues with resolution of inflammation (resolving tissues) did not cluster (**Figure 1*A***). Beside, a volcano plot revealed that the inflamed mucosa was significantly enriched in ω-6 AA-derived lipid mediators, in comparison with both healthy (**Figure 1*B***) and resolving tissues (**Figure 1*C***), with significantly reduced levels of lipid mediators derived from other precursors, including DHA-derived metabolites (**Figure 1*B and C***). We next evaluated the contribution of metabolites from the various lipid precursors to the total composition of lipid mediators. Results showed that while AA-derived metabolites were increased in active mucosa (**Figure 1*D and E***), the amount of docosanoids was significantly reduced (**Figure 1*D and F***), in comparison with healthy and remission groups, with no differences in the contribution of mediators from other lipid classes, such as EPA and LNA (**Supplementary Figure 1*A and B***). In line with previous evidences, reporting the high ω-

6/ω-3 fatty acid ratio to be an important player in the pathogenesis of many chronic diseases[15,16], we found the ratio of ω-6/ω-3 PUFA-derived metabolites significantly increased in active patients, versus healthy and resolving biopsies (**Figure 1*G***), thus confirming their inflammatory state. Overall, these results point out an impaired ω-3 pro-resolving metabolism in the inflamed mucosa, mainly due to a reduction in docosanoids.

MFSD2A in the gut localizes to the vascular endothelium and is up-regulated during resolution of intestinal inflammation

In order to understand the mechanism behind the reduced amount of ω-3 presolving lipid mediators observed in patients with active UC, we focused our attention on DHA-metabolism. The presence of MFSD2A and its correlation with DHA in the gut has never been characterized. Our results showed that in the human large intestine, MFSD2A mainly localizes to the endothelium, under both healthy (**Supplementary 1*C* and *D*)** and inflammatory conditions **(Figure 2*A* and *B***), with no expression in other cell types (**Figure 2*A,* 2*B*, Supplementary Figure 1*C* and *D***). This was confirmed on primary cultures of human intestinal microvascular endothelial cells (HIMECs), where the protein localizes to both the plasma membrane and the cytoplasm **(Supplementary Figure 1*C*)**. Moreover, MFSD2A in HIMECs mainly co-localize with the endoplasmic reticulum marker Calnexin (**Figure 2*C***).

We next quantified MFSD2A protein levels in both mucosal extracts and HIMECs of active UC patients and healthy subjects (**Supplementary Table 2** for patient characteristics). Results showed that MFSD2A is up-regulated in the inflamed mucosa, particularly on microvessels, in comparison with healthy tissues (**Supplementary Figure 1*E and F***); this was also confirmed in UC-HIMECs versus healthy cells (**Figure 2*D***). Interestingly, to verify whether and which inflammatory cytokines, known to activate endothelial cells[17], and to play a critical role in UC pathogenesis[18] were able to modulate MFSD2A in the inflammatory milieu, we stimulated healthy HIMECs with IL1β, IL17, IL23, TNFα, IL6, and IFNγ. TNFα was the most effective in up-regulating MFSD2A, while other interleukins and IFNγ had no effects (**Supplementary Figure1*G***). Because of the limited amount of tissue from endoscopic biopsies in remission, and the unavailability of surgical specimens from remitting UC patients undergoing surgery for other complications, we were unable to isolate HIMECs from subjects with resolution of gut inflammation. For this reason, subsequent analyses were performed on whole biopsies. Interestingly, MFSD2A was even more upregulated in patients with UC undergoing remission,

in comparison with healthy and active tissues (**Figure 2*E***). This suggests an involvement of MFSD2A in the resolving phase of intestinal inflammation and raises the question of why MFSD2A displays an intermediate expression levels in active tissues, when compared to healthy and patients in remission.

To answer this question, transcript levels of *MFSD2A* were measured at 2 time points in both healthy and UC-HIMECs, upon treatment with TNFα. Results showed that while in healthy endothelium *MFSD2A* is progressively upregulated by TNFα, in UC-HIMECs the transcript levels reached a peak at 8 hours that dropped off after 24 hours of stimulation (**Supplementary Figure 1*H***).

These findings demonstrate not only that inflammatory cytokines such as TNFα directly regulate MFSD2A expression, but most importantly that UC-HIMECs display a defect in the proper TNFα-dependent modulation of this protein.

MFSD2A overexpression confers anti-angiogenic properties and dampens the TNFα-induced inflammatory response in HIMECs

Because MFSD2A is mostly expressed on intestinal endothelial cells, we functionally characterized its role on HIMECs, performing gain- and loss-of function studies. Using a lentiviral strategy, HIMECs isolated from the intestinal mucosa of healthy surgical resections were transduced either with a lentivirus carrying a short hairpin RNA (shRNA) targeting MFSD2A (shMFSD2A, **Supplementary Figure 2*A-C***) or a GFP-tagged MFSD2A overexpressing vector (MFSD2A-OE, **Supplementary Figure 2*D-F***). Results showed that MFSD2A silencing stimulates *in vitro* angiogenic properties of HIMECs, in terms of increased capillary morphogenesis formation (**Figure 3*A and B***) and growth rate (**Figure 3*C***), compared to the scramble control. On the contrary, MFSD2A-OE cells displayed an anti-angiogenic phenotype (**Figure 3*D-F***), demonstrating a specific role for MFSD2A in regulating biological functions of the intestinal endothelium.

We next wondered whether MFSD2A could influence the response of HIMECs to an inflammatory stimulus, such as TNFα. Although MFSD2A expression is increased in patients with active UC (see Figure 2*D* and *E*) and is upregulated by inflammatory stimuli in healthy cells (see Supplementary Figure 1*G*), MFSD2A silencing exacerbated the endothelial TNFα-induced response, in comparison with treated control; this was confirmed not only in terms of an increase in inflammatory markers, such as *IL6*, *IL1B, IL8, IL18, IL12a, MCP1* and *COX2*[18]

(**Supplementary Figure 2*G***), but also as increased translocation of the P65 subunit of NF-κB into the nucleus[19] (**Supplementary Figure 2*H-J***). On the contrary, overexpression of MFSD2A abated the TNFα-induced inflammatory response, when compared to HIMECs carrying the control GFP plasmid (**Figure 3*G-J***). Furthermore, we observed MFSD2A modulation to affect *in vitro* HIMEC permeability, as assessed by transendothelial electrical resistance (TEER) measurements (**Figure 3*K and 3L)***. Of note, either MFSD2A silencing or overexpression did not modify levels of inflammatory cytokines, NF-κB translocation into the nucleus and TEER in untreated HIMECs (**Figure 3*G-L* and Supplementary Figure 2*G-J***). Altogether, this data demonstrates that MFSD2A controls the intestinal endothelial response to an inflammatory stimulus.

MFSD2A overexpression promotes CYP450-dependent epoxygenation of DHA

The anti-inflammatory effects elicited by MFSD2A overexpression may be related to its capability of interfering with DHA incorporation and/or metabolism. To verify this hypothesis, we first analyzed fatty acids in untreated and DHA-treated MFSD2A-OE and silenced HIMECs by gas chromatography. The fatty acid profile showed a significant DHA enrichment in MFSD2A-OE cells upon treatment with DHA, in comparison with GFP treated HIMECs (**Figure 4*A and B***). Conversely, MFSD2A silencing resulted in reduced DHA cell incorporation, compared with control (**Figure 4*A* and Supplementary Figure 3*A***), demonstrating an involvement of MFSD2A in the endothelial retention of free DHA. Notably, although UC-HIMECs showed increased amounts of MFSD2A versus healthy cells (Figure 2D), they did not display higher DHA enrichment (**Supplementary Figure 3*B***), suggesting an altered MFSD2A capability to increase DHA retention in the active endothelium.

To understand whether MFSD2A overexpression could also modulate DHA metabolism, we next performed a fatty acyl lipidomic analysis on healthy MFSD2A-OE and GFP HIMECs. The lipidomic profile revealed that the percentage of DHA-derived metabolites relative to total lipid mediators was significantly higher in MFSD2A-OE cells, in comparison with GFP controls (**Figure 4*C* and Supplementary Figure 3*C***). Moreover, a volcano plot showed that the only lipid mediators significantly upregulated in MFSD2A-OE cells were those derived from DHA (**Figure 4*D***). While AA-derived compounds were significantly reduced in MFSD2A-OE cells (**Figure 4*C, D* and Supplementary Figure 3*C*)**, mediators derived from other lipid precursors, such as EPA, LA, LNA, and DGLA did not change among the two experimental

groups (**Supplementary Figure 3*C***). These data indicate that MFSD2A overexpression modulates not only DHA retention in HIMECs, but also modifies its metabolism, thus mimicking the lipid mediator profile of resolving UC (Figure 1).

ω-3 DHA, ω-6 AA and other PUFAs can be metabolized by cyclooxygenases (COX), lipoxygenases (LOX) and cytochrome *P*450 (CYP) enzymes to a vast array of biologically active oxygenated lipid mediators[8,20]. The lipidomic profile of healthy MFSD2A-OE and GFP HIMECs revealed that among all oxylipins, only CYP450 epoxygenase-derived metabolites of DHA and AA were modulated in MFSD2A-OE versus GFP control cells (**Figure 4*E, F* and Supplementary Figure 3*D* and *E***). CYP450 converts PUFAs to epoxy lipid mediators including epoxyeicosatrienoic acids (EpETrEs) derived from AA and epoxydocosapentaenoic acids (EpDPEs) from DHA[7,8,21]. MFSD2A-OE HIMECs showed a decrease in the CYP450-derived EpETrEs of AA, in comparison with control cells, including their respective hydrolysis metabolites, the diols (DiHETrE), which are known to be biologically inactive[22] (**Figure 4*E and F***). Most importantly we found a significant burst of resolving EpDPEs from DHA in MFSD2A-OE cells, compared to GFP controls (**Figure 4*E and F***), indicating that high levels of MFSD2A promote CYP450 epoxygenation of DHA and relative resolving oxylipins. Of note, the effects of MFSD2A overexpression resembled the conditions observed in the resolving mucosa, where the amount of EpDPEs were increased compared to inflamed tissues (**Figure 4*G* and Supplementary Figure 3*F)***; vice versa, patients with active UC showed a significant increase in inflammatory COX- and LOX-derived AA metabolites[23], with no changes in CYP-derived lipid mediators, compared to healthy and patients in remission (**Supplementary Figure 3*G***), being consistent with the inflammatory milieu of damaged mucosa.

Reduced levels of DHA-derived epoxides in active mucosal biopsies compared to healthy controls were also observed in UC-HIMECs versus healthy cells (**Supplementary Figure 3*H and I***), revealing a selective defect in the endothelial production of EpDPEs. Importantly, this defect was not dependent on reduced basal levels of intracellular DHA (see Supplementary Figure 3*B*). Altogether, these findings reveal not only a specific role for MFSD2A in promoting DHA accretion and metabolism to EpDPEs in the gut endothelium, but also that these capabilities are impaired in the vasculature of active UC patients.

The resolving effects of MFSD2A-OE HIMECs are mediated by the production of CYP2C-derived DHA oxylipins

The main PUFA-metabolizing CYPs belong to the CYP2 family, in particular the CYP2J and CYP2C subfamilies, all localized in the endoplasmic reticulum (ER)[24]. The CYP2C subfamily represents one of the two major pieces of the intestinal P450 pie[25]. To verify whether the beneficial effects exerted by MFSD2A overexpression on HIMECs depends on its capability to promote CYP2C-derived metabolites of DHA, we first analyzed whether MFSD2A and CYP2C co-localized within the endoplasmic reticulum. The two proteins were indeed found in close proximity (**Figure 4*H***), but did not physically interact, as shown by co-immunoprecipitation studies (**Supplementary Figure 3*J***). We next inhibited CYP2C enzymes in MFSD2A-OE healthy HIMECs using Proadifen hydrochloride, a chemical agent known to be highly selective for the CYP-epoxygenase pathway[24]. Proadifen was able to abate the resolving effects exerted by MFSD2A overexpression in TNFα-treated HIMECs, in terms of increased TEER (**Figure 4*I***), and higher production of inflammatory cytokines and markers of endothelium activation (**Figure 4*J***). Importantly, the reduced amount of EpDPEs observed in UC-HIMECs is not due to reduced expression levels of *CYP2C* (**Supplementary Figure 3*K***), or to its enzymatic activity. In fact, epoxy metabolites derived from other lipid precursors, did not change between the two groups (**Supplementary Figure 3*L***). Collectively, this data demonstrates that MFSD2A controls angiogenic and resolving properties of the gut vasculature through modulation of CYP2C-dependent DHA epoxygenation. Consistently, when overexpressed in UC-HIMECs, MFSD2A restored not only the defective capability of these cells to promote DHA epoxygenation (**Supplementary Figure 4*A***), but also exerted anti-inflammatory effects, in terms of reduced *in vitro* capillary formation (**Supplementary Figure 4*B***) and production of inflammatory/angiogenic markers (**Supplementary Figure 4*C*).** We finally reasoned whether the limited amount of EpDPEs could be responsible for the hampered increase of TNFα-induced MFSD2A expression in UC-HIMECs. Experiments performed with healthy HIMECs in the presence or absence of Proadifen at 8 and 24 hours of TNFα stimulation demonstrated that CYP2C-dependent DHA epoxygenation controls the sustained levels of *MFSD2A* transcripts at later phases (24 hours), whereas is not responsible for the early upregulation (8 hours) (**Supplementary Figure 4*D***).

Transplantation of MFSD2A-OE ECFC in combination with DHA administration ameliorates DSS-induced acute colitis via CYP2C-dependent EpDPE production

The resolution process occurs during the acute phase of inflammation[26]. For this reason, to establish whether MFSD2A overexpression on endothelial cells could promote *in vivo* the resolution of intestinal inflammation, we choose the Dextran Sodium Sulfate (DSS)-induced model of acute colitis. Moreover, we took advantage of the capability of human endothelial colony-forming cells (ECFCs), to be recruited to ischemic or inflamed tissues[27], where they remodel the vascular compartment[28]. We transduced mCherry-tagged human ECFCs with MFSD2A-GFP-carrying lentiviral particles (ECFCs-MFSD2A) or GFP-expressing ECFCs (ECFCs-GFP), as control. CD1 nude mice undergoing DSS treatment for 6 days were then intravenously injected at day 5 with genetically modified ECFCs and monitored for the next 5 days. To enhance the potential of MFSD2A in promoting resolution of inflammation, parallel groups, of either ECFCs-GFP or -MFSD2A transplanted mice were gavaged with ethyl ester of DHA or water daily.

We first verified whether these cells were able to distribute from the peripheral blood to the inflamed mucosa of DSS-induced colitic mice[29]. Intravenously injected mCherry-positive human ECFCs (**Figure 5*A***) were indeed shown to home to the inflamed colon of immunedeficient mice with colitis (**Figure 5*B* and Supplementary 4*E***), with cells integrating either into pre-existing vessels (**Figure 5*C***) or into perivascular regions (**Figure 5*D***), as previously reported for other organs[30]. Interestingly, ECFCs were found to integrate only into blood vessels, and not into lymphatics (**Supplementary Figure 4*F***). Notably, no cell engraftment was observed in the intestine of healthy animals (**Supplementary Figure 4*G***). FACS analysis on large and small intestines, and on unrelated organs, revealed that while ECFCs were detectable at low levels also in the small intestine as well as the liver 2 weeks after transplantation, with a progressive decrease at later time points (**Supplementary Figure 5*A* and *B***), no cells were found in other unrelated organs at any time point (**Supplementary Figure 5*B***). ECFCs were still detectable 6 weeks after injection only in the colon in a small percentage (**Supplementary Figure 5*A* and *B***), indicating that their half-life is limited and could be used as a safe therapy. The transduction efficiency was confirmed by increased transcript levels of *MFSD2A* in ECFCs-MFSD2A cells compared to controls (**Supplementary Figure 5*C***).

Only delivery of ECFCs-MFSD2A in combination with DHA significantly reduced the severity of colitis, in comparison with the control group (only DSS); this was confirmed in terms of Disease Activity Index (DAI)[31] (**Figure 5*E***), endoscopic evaluation (**Figure 5*F* and**

Supplementary Figure 5*D*), colon length (**Supplementary Figure 5*E***), decreased inflammatory markers (**Supplementary Figure 5*F***), and reduced infiltration of neutrophils (**Supplementary Figure 5*G***) .

Angiogenesis, increased expression of adhesion molecules (e.g. VCAM1, MadCam1), angiogenic markers (VEGFA, Nos2, Angiopoietin 1), and altered vascular permeability are all features of an activated endothelium[32]**,** which are also observed during intestinal inflammation[33]**.** Only delivery of ECFCs-MFSD2A in combination with DHA administration was able to reduce the expression levels of these markers (**Figure 5*G***), and only this experimental group showed reduced vascular permeability, as revealed by decreased fluorescence intensity of Plasmalemmal vesicle-1 (PV1) on endothelial cells[34] (**Figure 5*H* and Supplementary Figure 5*H***), and reduced size of hematic vessels (**Supplementary Figure 5*I***).

Finally, lipidomic analysis performed on the colons of all experimental groups, showed a significant up-regulation of docosanoids only in DHA-fed mice transplanted with ECFCs-MFSD2A (**Supplementary Figure 6*A***). In these mice, only EpDPEs were found significantly increased among all DHA metabolites, with no major modifications for oxylipins derived from other PUFAs (**Figure 5*I* and Supplementary Figure 6*B-D***). Treating mice with Proadifen in order to inhibit the production of resolving EpDPEs (**Figure 6*A* and Supplementary Figure 6*E***), resulted in the reversion of clinical parameters (**Figure 6B and 6C**), and anti-angiogenic phenotype (**Figure 6*D and E***). Notably, beneficial effects of ECFCs-MFSD2A in DHA-fed transplanted mice were retained also in the DSS-induced chronic model of colitis, in terms of reduced DAI (**Figure 6*F***), endoscopic score (**Figure 6*G***), low PV-1 expression on endothelial cells (**Figure 6*H***) and diminished recruitment of neutrophils in the inflamed colon (**Figure 6*I***), compared to the other groups. This is consistent with the fact that ECFCs were still detected 4 weeks after injection (see Supplementary Figure 5*A* and *B*) and support the significance of a long-lived effect of ECFCs-MFSD2A cargo on the course of colitis.

Overall, these findings show that delivery of *MFSD2A* through a cell-based therapy in combination with DHA oral supplementation dampens both acute and chronic colitis via production of CYP2C-dependent resolving EpDPEs. Remarkably, administration of single EpDPEs did not show any beneficial effects on mice with colitis (**Supplementary Figure 7*A and B***).

Discussion

Because the gut is regarded as being in a state of controlled inflammation[35], an effective resolution program is fundamental to prevent chronic tissue damage, and it is reasonable to assume that defective expression of resolving mediators, along with prolonged endothelial activation[9] may contribute to the chronic inflammatory response associated with UC. Previous studies have foreseen this concept, showing lower levels of EPA and DHA lipid precursors with higher levels of AA in mucosa of patients with UC[36]. Here we provide the first evidence that patients with active UC fail in producing resolving metabolites derived from DHA epoxygenation, and that these lipid mediators are highly present in patients with UC undergoing remission, thus revealing their role in the resolution of intestinal inflammation. Most importantly, we found that MFSD2A is required for both DHA retention and metabolism in the healthy gut vasculature, thus modulating endothelial capabilities to properly respond to an inflammatory stimulus; however these functions are impaired in UC-HIMECs, resulting in reduced generation of EpDPEs.

To date MFSD2A has mostly been studied for its role as transporter of common plasma LysoPCs carrying long-chain polyunsaturated fatty acids in the brain, placenta and retina, with particular attention to DHA[12,14,37]. In this work, we show MFSD2A in the gut to be exclusively expressed in the endothelium and to control important biological functions of the intestinal vasculature, including its ability to mount a proper anti-inflammatory response. Moreover, we demonstrate that the generation of EpDPEs and the beneficial effects exerted by *MFSD2A* overexpression, are mediated both *in vivo* and *in vitro* by CYP2C, one of the major isoforms of the CYP450 family expressed in the intestine[25], that co-localize with MFSD2A in the endoplasmic reticulum. This is consistent with the notion that ω-3 fatty acids are poor substrates of COX and LOX enzymes[38], whereas they are highly efficient alternative substrates for numerous isoforms of CYP epoxygenases[39].

The interest in ω-3 PUFAs as a source of biosynthetic products during the resolution of inflammation has grown tremendously, and their use has been practiced for both prevention and treatment of different inflammatory diseases, in animals and humans[40]. Nevertheless, while few clinical studies involving the administration of DHA and EPA showed some efficacy in the course of UC, most of them have given rise to inconclusive or negative results[41]. Our findings provide an explanation for this discrepancy by showing that a selected cohort of not responding patients with UC owns a dysfunctional MFSD2A in the gut endothelium.

Recent pre-clinical studies have demonstrated that newly identified DHA-derived metabolites from LOX enzymatic pathway, such as Maresin 1, Resolvin D2, and aspirin-triggered Resolvin D1[42,43], as well as RvE1 from EPA[44,45], are quite effective in preventing intestinal inflammation. Unlike these findings, we did not observe beneficial effects with any of the DHA-derived epoxides used to treat experimental colitis, including treatment with DHA alone. This discrepancy may be due to several reasons: 1) a different treatment regimen; while most of the studies treat mice with a "prevention" regimen, we administered single EpDPEs only once colitis was fully established; 2) the epoxides we added may have not reached the site of action compared to the endogenously generated compounds. While these are theories, the fact that DHA metabolites help to reduce inflammation and the only products that are distinctly generated are the EpDPEs, strongly argues for their role.

Notably, we found *MFSD2A* to be strongly increased by TNFα in healthy HIMECs in two distinct phases: an "early phase", corresponding to the onset of inflammation, where the inflammatory milieu containing TNFα triggers *MFSD2A* expression, and a "late phase", corresponding to the onset of resolution, where MFSD2A-dependent generation of EpDPEs not only helps to resolve inflammation, but induces a positive-feedback loop that further increases the transcript levels of *MFSD2A*. In UC-HIMECs this positive loop fails to occur, because of the altered capability of MFSD2A in promoting DHA retention and metabolism. This might justify why subjects with active UC display intermediate *MFSD2A* levels compared to the other groups, leading to an unsuccessful resolution program (see schematic representation in **Figure 7*A***).

In an attempt to translate our findings into clinical management of UC, we overexpressed functional MFSD2A in UC-HIMECs, where it was able to rescue the defective capability of these cells in triggering a proper resolution program. Furthermore, we delivered MFSD2A as "therapeutic" gene in the DSS-induced experimental models of colitis, using ECFCs. Compared with mature endothelial cells that possess limited regenerative capacity[46], ECFCs are endowed with high proliferative potential and robust vasculogenic properties that render these cells a promising opportunity for clinical use[47]. Our pre-clinical approach allowed ECFCs-MFSD2A to increase *in situ* EpDPE production, which in turn showed inhibitory effects on angiogenesis, vascular permeability and expression of inflammatory cytokines, thus leading to the clinical amelioration of intestinal inflammation (**Figure 7*B***).

The mechanism through which MFSD2A promotes CYP2C-dependent epoxygenation of DHA in intestinal endothelial cells needs further investigation. In fact, MFSD2A is not considered a transporter of unesterified DHA, but only of DHA-containing lysophosphatidylcholine (LysoPC-DHA). Our *in vitro* experiments have been performed using unesterified DHA. We believe free DHA may enter the cell via an MFSD2A-independent mechanism[48]; once inside, it may be incorporated into membrane phospholipids of the endoplasmic reticulum[49], where MFSD2A in close proximity with CYP2C helps this enzyme to metabolize DHA.

Studies regarding the mechanisms behind the resolution process involved in UC pathogenesis are still at their early stages. Our work presents not only the first evidence that patients with UC display insufficient production of resolving DHA epoxides, but describes a novel, significant role for MFSD2A in the maintenance of an effective resolution program. Moreover, we provide not only important insights into the molecular mechanisms regulating resolution of intestinal inflammation, but also a strong rationale for the development of novel therapeutic strategies to treat UC. Because drug therapy, diet and lifestyle changes do not always relieve signs and symptoms of this disease, our cell-based therapeutic approach may help a selective cohort of non-responding patients, with the potential advantage of avoiding immune suppression, and using natural endogenous pathways to resolve inflammation.

References

1. Danese S, Fiocchi C. Ulcerative Colitis. N Engl J Med 2011;365:1713–1725.
2. Das UN. Inflammatory bowel disease as a disorder of an imbalance between pro- and anti-inflammatory molecules and deficiency of resolution bioactive lipids. Lipids Health Dis 2016;15:11.
3. Shores DR, Binion DG, Freeman BA, et al. New insights into the role of fatty acids in the pathogenesis and resolution of inflammatory bowel disease. Inflamm Bowel Dis 2011;17:2192–204. .
4. Serhan CN, Chiang N, Dalli J. The resolution code of acute inflammation: Novel pro-resolving lipid mediators in resolution. Semin Immunol 2015.
5. Sugimoto MA, Sousa LP, Pinho V, et al. Resolution of Inflammation: What Controls Its Onset? Front Immunol 2016;7.

6. Calder PC. Polyunsaturated fatty acids, inflammatory processes and inflammatory bowel diseases. Mol Nutr Food Res 2008;52:885–97.
7. Spector AA, Kim H-Y. Cytochrome P450 epoxygenase pathway of polyunsaturated fatty acid metabolism. Biochim Biophys Acta 2015;1851:356–65.
8. Zhang G, Kodani S, Hammock BD. Stabilized epoxygenated fatty acids regulate inflammation, pain, angiogenesis and cancer. Prog Lipid Res 2014;53:108–23.
9. Danese S, Fiocchi C. Endothelial Cell-Immune Cell Interaction in IBD. Dig Dis 2016;34:43–50.
10. Liebert MA, Kadl A, Leitinger N. The Role of Endothelial Cells in the Resolution of Acute Inflammation OF LEUKOCYTE ADHESION. 2005;7:1744–1754.
11. Harvey KA, Xu Z, Pavlina TM, et al. Modulation of endothelial cell integrity and inflammatory activation by commercial lipid emulsions. Lipids Health Dis 2015;14:9.
12. Nguyen LN, Ma D, Shui G, et al. Mfsd2a is a transporter for the essential omega-3 fatty acid docosahexaenoic acid. Nature 2014;509:503–6.
13. Quek DQY, Nguyen LN, Fan H, et al. Structural insights into the transport mechanism of the human sodium-dependent lysophosphatidylcholine transporter Mfsd2a. J Biol Chem 2016.
14. Wong BH, Chan JP, Cazenave-Gassiot A, et al. Mfsd2a is a transporter for the essential omega-3 fatty acid DHA in eye and important for photoreceptor cell development. J Biol Chem 2016.
15. Marion-Letellier R, Savoye G, Ghosh S. Polyunsaturated fatty acids and inflammation. IUBMB Life 2015;67:659–667.
16. Simopoulos A. An Increase in the Omega-6/Omega-3 Fatty Acid Ratio Increases the Risk for Obesity. Nutrients 2016;8:128.
17. Madge LA, Pober JS. TNF signaling in vascular endothelial cells. Exp Mol Pathol 2001;70:317–25.
18. Neurath MF. Cytokines in inflammatory bowel disease. Nat Rev Immunol 2014;14:329–342.
19. Kempe S. NF- B controls the global pro-inflammatory response in endothelial cells: evidence for the regulation of a pro-atherogenic program. Nucleic Acids Res 2005;33:5308–5319.
20. Wijendran V, Hayes KC. Dietary n-6 and n-3 fatty acid balance and cardiovascular

health. Annu Rev Nutr 2004;24:597–615.

21. Yanai R, Mulki L, Hasegawa E, et al. Cytochrome P450-generated metabolites derived from ω-3 fatty acids attenuate neovascularization. Proc Natl Acad Sci U S A 2014;111:9603–8.
22. Zeldin DC, Wei S, Falck JR, et al. Metabolism of epoxyeicosatrienoic acids by cytosolic epoxide hydrolase: substrate structural determinants of asymmetric catalysis. Arch Biochem Biophys 1995;316:443–51.
23. Calder PC. Long-chain polyunsaturated fatty acids and inflammation. Scand J Food Nutr 2006;50:54–61.
24. Gilroy DW, Edin ML, Maeyer RPH De, et al. CYP450-derived oxylipins mediate inflammatory resolution. Proc Natl Acad Sci U S A 2016;113:E3240-9.
25. Paine MF, Hart HL, Ludington SS, et al. The human intestinal cytochrome P450 “pie”. Drug Metab Dispos 2006;34:880–6.
26. Headland SE, Norling L V. The resolution of inflammation: Principles and challenges. Semin Immunol 2015.
27. Goto K, Takemura G, Takahashi T, et al. Intravenous Administration of Endothelial Colony-Forming Cells Overexpressing Integrin β1 Augments Angiogenesis in Ischemic Legs. Stem Cells Transl Med 2016;5:218–26.
28. Wood JA, Colletti E, Mead LE, et al. Distinct contribution of human cord blood-derived endothelial colony forming cells to liver and gut in a fetal sheep model. Hepatology 2012;56:1086–96.
29. Chassaing B, Aitken JD, Malleshappa M, et al. Dextran Sulfate Sodium (DSS)-Induced Colitis in Mice. In: *Current Protocols in Immunology*. Hoboken, NJ, USA: John Wiley & Sons, Inc.; 2014:15.25.1-15.25.14.
30. Dome B, Dobos J, Tovari J, et al. Circulating bone marrow-derived endothelial progenitor cells: Characterization, mobilization, and therapeutic considerations in malignant disease. Cytom Part A 2008;73A:186–193.
31. Randhawa PK, Singh K, Singh N, et al. A Review on Chemical-Induced Inflammatory Bowel Disease Models in Rodents. Korean J Physiol Pharmacol 2014;18:279.
32. Pober JS, Sessa WC. Evolving functions of endothelial cells in inflammation. Nat Rev Immunol 2007;7:803–15.
33. Scaldaferri F, Vetrano S, Sans M, et al. VEGF-A links angiogenesis and inflammation in

inflammatory bowel disease pathogenesis. Gastroenterology 2009;136:585–95.e5.
34. Spadoni I, Zagato E, Bertocchi A, et al. A gut-vascular barrier controls the systemic dissemination of bacteria. Science 2015;350:830–4.
35. Maloy KJ, Powrie F. Intestinal homeostasis and its breakdown in inflammatory bowel disease. Nature 2011;474:298–306.
36. Masoodi M, Pearl DS, Eiden M, et al. Altered colonic mucosal Polyunsaturated Fatty Acid (PUFA) derived lipid mediators in ulcerative colitis: new insight into relationship with disease activity and pathophysiology. PLoS One 2013;8:e76532.
37. Prieto-Sánchez MT, Ruiz-Palacios M, Blanco-Carnero JE, et al. Placental MFSD2a transporter is related to decreased DHA in cord blood of women with treated gestational diabetes. Clin Nutr 2016.
38. Jump DB. The Biochemistry of n-3 Polyunsaturated Fatty Acids. J Biol Chem 2002;277:8755–8758.
39. Arnold C, Markovic M, Blossey K, et al. Arachidonic acid-metabolizing cytochrome P450 enzymes are targets of {omega}-3 fatty acids. J Biol Chem 2010;285:32720–33.
40. Calder PC. Omega-3 polyunsaturated fatty acids and inflammatory processes: nutrition or pharmacology? Br J Clin Pharmacol 2013;75:645–62.
41. Barbalho SM, Goulart R de A, Quesada K, et al. Inflammatory bowel disease: can omega-3 fatty acids really help? Ann Gastroenterol Q Publ Hell Soc Gastroenterol 29:37–43.
42. Bento AF, Claudino RF, Dutra RC, et al. Omega-3 fatty acid-derived mediators 17(R)-hydroxy docosahexaenoic acid, aspirin-triggered resolvin D1 and resolvin D2 prevent experimental colitis in mice. J Immunol 2011;187:1957–69
43. Marcon R, Bento AF, Dutra RC, et al. Maresin 1, a proresolving lipid mediator derived from omega-3 polyunsaturated fatty acids, exerts protective actions in murine models of colitis. J Immunol 2013;191:4288–98.
44. Arita M, Yoshida M, Hong S, et al. Resolvin E1, an endogenous lipid mediator derived from omega-3 eicosapentaenoic acid, protects against 2,4,6-trinitrobenzene sulfonic acid-induced colitis. Proc Natl Acad Sci U S A 2005;102:7671–6.
45. Ishida T, Yoshida M, Arita M, et al. Resolvin E1, an endogenous lipid mediator derived from eicosapentaenoic acid, prevents dextran sulfate sodium-induced colitis. Inflamm Bowel Dis 2010;16:87–95.

46. Lee PSS. Endothelial progenitor cells in cardiovascular diseases. World J Stem Cells 2014;6:355.
47. Melero-Martin JM, Obaldia ME De, Kang S-Y, et al. Engineering Robust and Functional Vascular Networks In Vivo With Human Adult and Cord Blood-Derived Progenitor Cells. Circ Res 2008;103:194–202.
48. Pan Y, Scanlon MJ, Owada Y, et al. Fatty Acid-Binding Protein 5 Facilitates the Blood-Brain Barrier Transport of Docosahexaenoic Acid. Mol Pharm 2015;12:4375–85.
49. Kim H-Y. Novel Metabolism of Docosahexaenoic Acid in Neural Cells. J Biol Chem 2007;282:18661–18665.

Figure Legends

Figure 1. LC-MS/MS analysis performed on endoscopic mucosal biopsies reveals a defined lipid signature in patients with UC.

(*A*) Principal component analysis (PCA) of LC-MS/MS data from healthy, active and patients in remission (n=9/group).

(*B* and *C*) Volcano plot showing statistical significance (y-axis) as a function of the fold change (FC, x-axis) in fatty acid class production of active versus healthy (B) and active versus remission (C) (n=9/group).

(*D*) Heat map showing significant variations of AA- and DHA-derived metabolites over total lipid mediators among healthy, active and patients in remission (n=9/group).

(*E* and *F*) Percentage variations of AA- (E) and DHA- (F) metabolites over total LC-MS/MS-detected fatty acyl lipids (FA) (n=9/group).

(*G*) Ratio of the percentage of ω-6/ω-3 PUFA-derived lipid mediators in healthy, active and patients under remission (n=9/group).

*P < 0,05 and ***P < 0,005. Data are represented as mean ±s.e.m.

Figure 2. MFSD2A is exclusively expressed on human gut vasculature and is up-regulated during remission

(*A*) Representative images (n=5 images/colon) of sectioned human UC colons (n=8 subjects) stained for MFSD2A, VE-Cadherin (VE-Cad), α-Smooth Muscle Actin (αSMA), Junction adhesion molecule (JAM-A), and DAPI (blue).

(*B*) Representative images of tissues described in (A), stained for MFSD2A, CD68, CD11c, CD20 and CD3, DAPI (blue).

(*C*) Representative confocal images of healthy HIMECs stained for MFSD2A, the endoplasmic reticulum marker CALNEXIN and DAPI (blue).

(*D, top*) Western blot analysis of protein extracts from healthy and UC-HIMECs (active) (n=5/group). (*D, bottom*) Representative blots.

(*E, top*) Western blot analysis of protein extracts from endoscopic biopsies of healthy (n=4), active (n=8) and (n=7) remitting (remission) patients.

*P < 0,05; **P < 0,01. Scale bars, 50 µm for tissues, and 10 µm for HIMECs. All data are represented as mean ±s.e.m.

Figure 3. MFSD2A modulates angiogenic properties and TNFα-induced response of HIMECs

(*A* and *D*) Representative immunofluorescence of transduced HIMECs forming tubules stained for DAPI (blue) and GFP (green). Scale bars, 20 µm.

(*B* and *E*) Tubule quantification of shMFSD2A, MFSD2A-OE and relative control HIMECs at 4 and 6 hours after plating. n=3 replicates/condition/time point of 3 independent experiments.

(*C* and *F*) Proliferation of shMFSD2A, MFSD2A-OE and relative control HIMECs represented as optical density versus day 0, at the indicated time points. n=6 replicates/group of 3 independent experiments.

(*G*) Expression profile of inflammatory markers in untreated and TNFα-stimulated MFSD2A-OE and relative control HIMECs by qRT-PCR (n=3 replicates/condition of 5 independent experiments; # refers to untreated GFP vs TNFα-treated GFP; $ refers to untreated MFSD2A-OE vs TNFα-treated MFSD2A-OE).

(*H, top*) Western blot quantification of NF-κB-p65 subunit in nuclear and cytosolic protein extracts of unstimulated and TNFα-treated MFSD2A-OE and GFP HIMECs (n=3 replicates/condition of 3 independent experiments).

(*H, bottom*) Representative blots.

(*I*) Representative immunofluorescence of untreated and TNFα-stimulated MFSD2A-OE and GFP control HIMECs stained for NF-κB p65, GFP, and DAPI (blue). Scale bars, 20 µm.

(*J*) Quantification of NF-κB $p65^{+}$ nuclei expressed as percentage over total nuclei (n=3 replicates/condition of 3 independent experiments).

(*K* and *L*) TEER measurements of TNFα-stimulated shCTRL and shMFSD2A (K) and GFP and MFSD2A-OE (L) HIMECs (n=5 replicates/condition of 2 independent experiments).

*P < 0,05; **P < 0,01; ***P < 0,005; $^{\#}$P < 0,005; $^{\$}$P; < 0,005; $^{\&}$P < 0,005; $^{£}$P < 0,005. All data are represented as mean ±s.e.m.

Figure 4. MFSD2A overexpression promotes DHA retention and DHA epoxygenation in healthy HIMECs

(*A*) Graph representing µg of DHA/mg protein in shMFSD2A, MFSD2A-OE and relative control HIMECs with or without DHA treatment (n=3 replicates/condition of 2 independent experiments).

(*B*) Table listing µg of fatty acids/mg protein detected by gas-chromatography of MFSD2A-OE and GFP HIMECs with or without DHA (n=3 replicates/condition of 2 independent experiments;* refers to DHA-treated vs untreated; # refers to DHA-treated MFSD2A-OE vs DHA-treated GFP).

(*C*) Lipid composition by LC-MS/MS expressed in percentage of PUFA-derived lipid mediators over total fatty acids (FA) in MFSD2A-OE and GFP HIMECs (n=3/group).

(*D*) Volcano plot showing statistical significance (y-axis) as a function of the fold change (FC, x-axis) in PUFA-derived metabolites of MFSD2A-OE versus GFP HIMECs analyzed by LC-MS/MS (n=3/group).

(*E*) Heat map showing variations of PUFA-derived metabolites analyzed by LC-MS/MS in MFSD2A-OE and GFP control HIMECs (n=3/group). Empty squares represent CYP450-derived metabolites of AA and DHA.

(*F*) Percentage of CYP450-derived metabolites of AA, DHA, EPA and LA over total fatty acids (FA) in MFSD2A-OE and GFP HIMECs (n=3/group).

(*G*) Percentage of CYP450- and LOX-derived metabolites of DHA over total fatty acids (FA) detected by LC-MS/MS in endoscopic mucosal biopsies of healthy, active and remitting patients (n=9/group).

(*H*) Representative confocal images of healthy HIMECs stained for MFSD2A, CYP2C, and DAPI (blue). White arrows indicate co-localization of MFSD2A with CYP2C. Scale bar, 10 µm.

(*I*) TEER measurements of TNFα-stimulated MFSD2A-OE and GFP HIMECs with or without Proadifen (n=5 replicates of 2 independent experiments).

(*J*) Inflammatory cytokine and angiogenic factor expression profile of TNFα-stimulated MFSD2A-OE and GFP HIMECs with or without Proadifen by qRT-PCR (n=3 replicates for 2 independent experiments).

*P < 0,05; **P < 0,01; ***P < 0,005; $^{\#}$P <0,05. All data are represented as mean ±s.e.m.

Figure 5. Human ECFCs overexpressing MFSD2A promote *in vivo* DHA epoxygenation and ameliorates DSS-induced experimental colitis

(*A*) ECFCs isolated from human blood, and transduced with MFSD2A-OE/mCherry or GFP/mCherry control lentiviruses were intravenously injected in CD1 nude mice with colitis.

(*B*) Representative pictures of live imaging of a mouse with colitis (left) and isolated colons (right) at the indicated conditions one week after injection (n=2 independent experiments with 5 mice/group).

(*C* and *D*) 3D reconstruction of immunofluorescence (bottom) of frozen colons from ECFCs-GFP/mCherry-injected colitic mice one week after injection, stained for murine CD31 and visualized for mCherry (C) and GFP (D). (Top, red cells) Schematic representations of ECFCs integrated into mouse pre-existing vessels (C) and perivascular regions (D) (n=2 independent experiments with 5 mice/group).

(*E*) DAI of ECFCs-MFSD2A-injected DHA-fed colitic mice and control groups (n=2 independent experiments with 5 mice/group). (* refers to DSS only vs ECFCs-MFSD2A+DHA; # refers to ECFCs-MFSD2A vs ECFCs-MFSD2A+DHA; & refers to ECFCs-GFP+DHA vs ECFCs-MFSD2A+DHA).

(*F*) Representative endoscopic images (top) and 3D reconstruction of immunofluorescence of colons (bottom) stained for murine CD31, GFP-tagged MFSD2A, and DAPI (blue), from ECFCs-MFSD2A-injected DHA-fed colitic mice at the indicated conditions 5 days after ECFC transplantation. Scale bars, 10 µm (n=2 independent experiments with 5 mice/group).

(*G* and *H*) Quantification of angiogenic factors by qRT-PCR (G) and PV-1 mean fluorescence intensity (MFI)/vessel area (µm2) (H) in colons of ECFCs-MFSD2A-injected DHA-fed colitic mice at the indicated conditions, 5 days after injection (n=2 independent experiments with 5 mice/group).

(*I*) Heat map showing variation of PUFA-derived lipid mediators detected by LC-MS/MS in colon tissues of ECFCs-MFSD2A-injected DHA-fed colitic mice at the indicated conditions 3 days after ECFC injection (n=3 mice/group representative of 2 independent experiments). Empty square indicates CYP450-derived metabolites of DHA.

*P < 0,05; **P < 0,01; ***P < 0,005; $^{\#}$P < 0,05; $^{\#\#}$P < 0,01; $^{\&}$P < 0,05; $^{\&\&}$P < 0,01. All data are represented as mean ±s.e.m.

Figure 6. CYP2C inhibition abolishes resolving effects of human ECFCs-MFSD2A transplantation during experimental colitis

(*A*) Heat map showing variations of CYP450-derived metabolites, detected by LC-MS/MS in colons of ECFCs-MFSD2A-injected DHA-fed colitic mice at the indicated conditions 3 days after injection (n=3 mice/group for 2 independent experiments). Empty square indicates DHA epoxides.

(*B*) DAI of ECFCs-MFSD2A-injected DHA-fed colitic mice and control groups with or without Proadifen administration (n=2 independent experiments with 5 mice per group; * refers to DSS only vs ECFCs-MFSD2A+DHA; # refers to ECFCs-MFSD2A vs ECFCs-MFSD2A+DHA; & refers to ECFCs-GFP+DHA vs ECFCs-MFSD2A+DHA; $ refers to ECFCs-MFSD2A+DHA vs ECFCs-MFSD2A+DHA with Proadifen.

(*C-E*) Colon length (C), inflammatory and angiogenic expression profile by qRT-PCR (D) and quantification of PV-1 mean fluorescence intensity (MFI)/vessel area (μm^2) (E) of colons from ECFCs-MFSD2A-injected DHA-fed colitic mice at the indicated conditions 5 days after ECFC injection (n=2 independent experiments with 5 mice/group).

(*F*) DAI of ECFCs-MFSD2A-injected DHA-fed colitic mice and control groups in a DSS-induced chronic model of colitis. n=2 independent experiments with 5 mice/group; * refers to DSS only vs ECFCs-MFSD2A+DHA; # refers to ECFCs-MFSD2A vs ECFCs-MFSD2A+DHA; $ refers to ECFCs-GFP+DHA vs ECFCs-MFSD2A+DHA.

(*G-I*) Endoscopic score (G), quantification of PV-1 mean fluorescence intensity (MFI)/vessel area (μm^2) (H) and $Ly6G^+$ cell infiltration (neutrophils) (I) of colons isolated from ECFCs-MFSD2A-injected DHA-fed colitic mice at the indicated conditions (n=2 independent experiments with 5 mice/group).

*P and $^{\&}$P < 0,05; **P < 0,01; ***P < 0,005; $^{\#}$P < 0,05; $^{\#\#}$P < 0,01, $^{\$}$P < 0,05, $^{\$\$}$P <0,01, $^{\$\$\$}$P <0,005. All data are represented as ±s.e.m.

Figure 7. MFSD2A promotes CYP2C-dependent epoxygenation of DHA in endothelial cells to generate pro-resolving metabolites and dampen intestinal inflammation

(*A*) The inflammatory milieu in the acute phase of patients with UC (a) promotes early *MFSD2A* upregulation. During the onset of resolution (b), MFSD2A efficiently triggers EpDPE generation only in patients with UC in remission (green arrow). This leads to late up-regulation of the protein (yellow arrow), that in turn sustains DHA epoxidation (red arrow) and resolution of inflammation (c). In patients with active UC the absence of a positive-feedback loop between MFSD2A and DHA epoxides leads to chronic inflammation (d).

(*B*) ECFCs-MFSD2A transplanted in mice with colitis, in combination with oral DHA administration, home to the inflamed mucosa, integrate either into pre-existing vessels or into perivascular regions and promote the release of DHA epoxy metabolites; this stimulates the reduction of inflammatory cytokines, angiogenesis and vascular permeability, thus triggering the resolution program. (Servier Medical Art, www.servier.com).

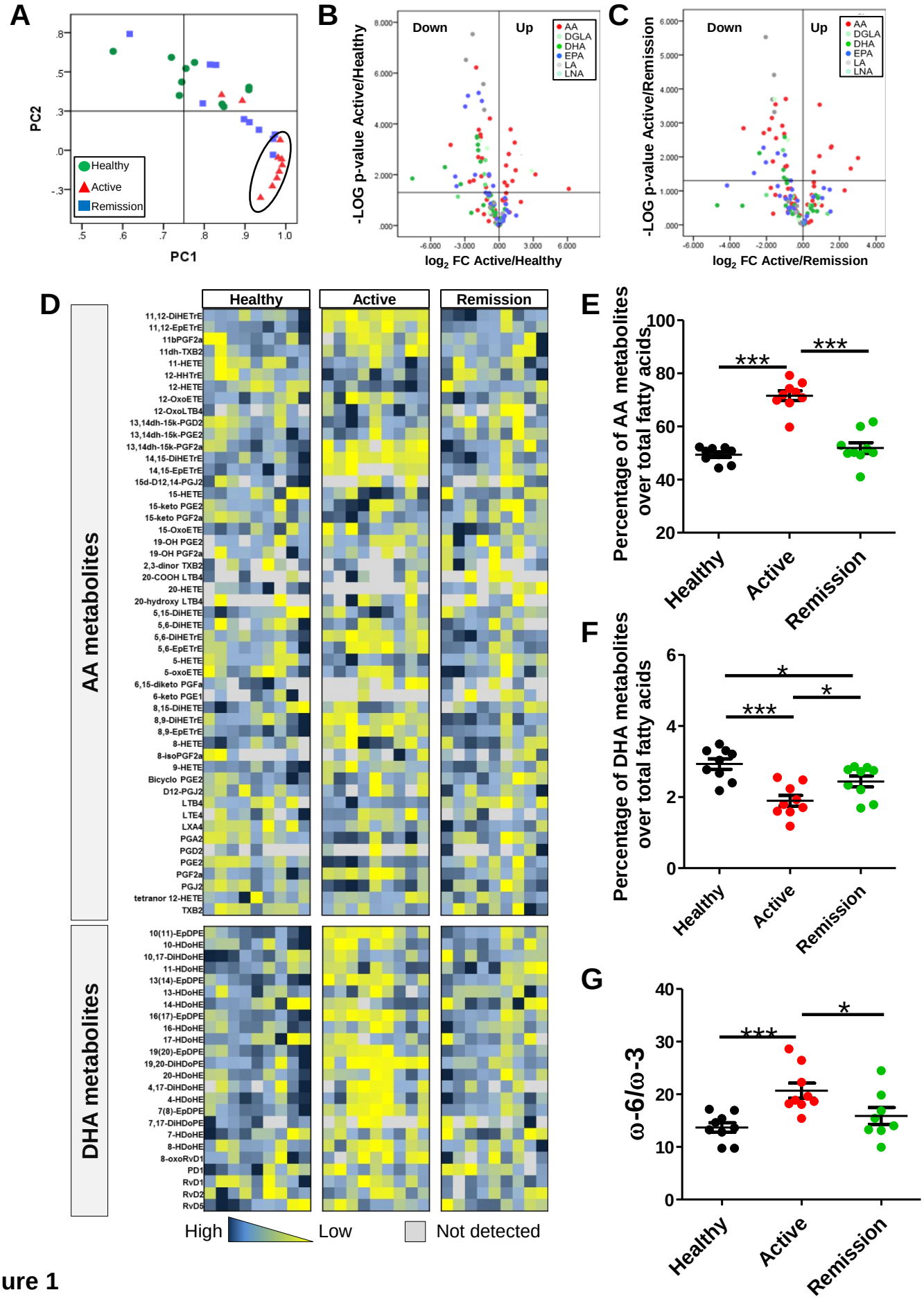
A
PC2
PC1
Healthy
Active
Remission
B
Down
Up
AA
DGLA
DHA
EPA
LA
LNA
-LOG p-value Active/Healthy
log2 FC Active/Healthy
C
Down
Up
-LOG p-value Active/Remission
log2 FC Active/Remission
D
Healthy
Active
Remission
AA metabolites
DHA metabolites
11,12-DiHETrE
11,12-EpETrE
11bPGF2a
11dh-TXB2
11-HETE
12-HHTrE
12-HETE
12-OxoETE
12-OxoLTB4
13,14dh-15k-PGD2
13,14dh-15k-PGE2
13,14dh-15k-PGF2a
14,15-DiHETrE
14,15-EpETrE
15d-D12,14-PGJ2
15-HETE
15-keto PGE2
15-keto PGF2a
15-OxoETE
19-OH PGE2
19-OH PGF2a
2,3-dinor TXB2
20-COOH LTB4
20-HETE
20-hydroxy LTB4
5,15-DiHETE
5,6-DiHETE
5,6-DiHETrE
5,6-EpETrE
5-HETE
5-oxoETE
6,15-diketo PGFa
6-keto PGE1
8,15-DiHETE
8,9-DiHETrE
8,9-EpETrE
8-HETE
8-isoPGF2a
9-HETE
Bicyclo PGE2
D12-PGJ2
LTB4
LTE4
LXA4
PGA2
PGD2
PGE2
PGF2a
PGJ2
tetranor 12-HETE
TXB2
10(11)-EpDPE
10-HDoHE
10,17-DiHDoHE
11-HDoHE
13(14)-EpDPE
13-HDoHE
14-HDoHE
16(17)-EpDPE
16-HDoHE
17-HDoHE
19(20)-EpDPE
19,20-DiHDoPE
20-HDoHE
4,17-DiHDoHE
4-HDoHE
7(8)-EpDPE
7,17-DiHDoPE
7-HDoHE
8-HDoHE
8-oxoRvD1
PD1
RvD1
RvD2
RvD5
High
Low
Not detected
E
Percentage of AA metabolites over total fatty acids
***
***
Healthy
Active
Remission
F
Percentage of DHA metabolites over total fatty acids
*
*
***
Healthy
Active
Remission
G
ω-6/ω-3
***
*
Healthy
Active
Remission

Figure 1

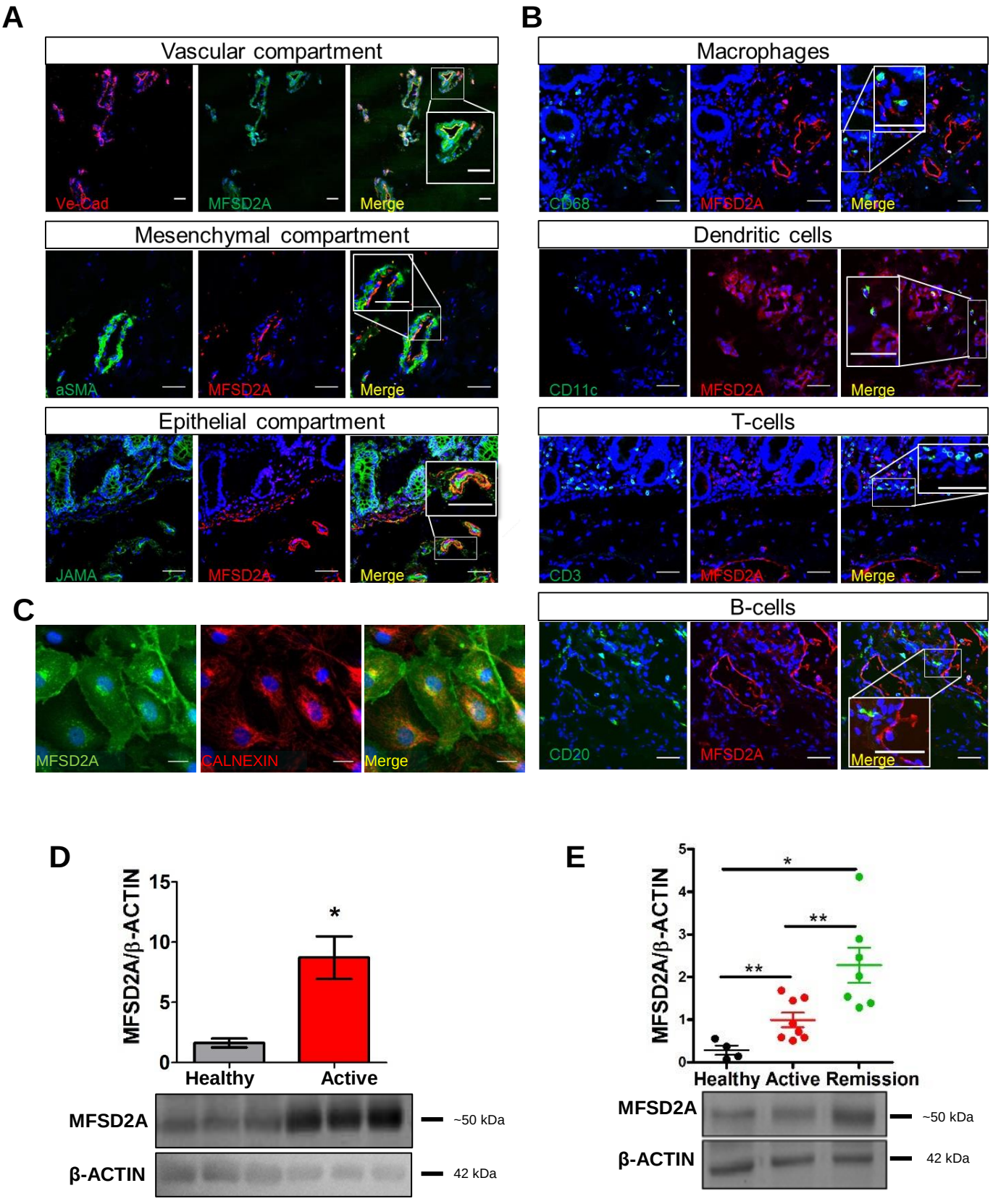
A
Vascular compartment
Ve-Cad
MFSD2A
Merge
Mesenchymal compartment
aSMA
MFSD2A
Merge
Epithelial compartment
JAMA
MFSD2A
Merge
B
Macrophages
CD68
MFSD2A
Merge
Dendritic cells
CD11c
MFSD2A
Merge
T-cells
CD3
MFSD2A
Merge
B-cells
CD20
MFSD2A
Merge
C
MFSD2A
CALNEXIN
Merge
D
MFSD2A/β-ACTIN
15
10
5
0
*
Healthy
Active
MFSD2A
β-ACTIN
~50 kDa
42 kDa
E
MFSD2A/β-ACTIN
5
4
3
2
1
0
*
**
**
Healthy Active Remission
MFSD2A
β-ACTIN
~50 kDa
42 kDa

Figure 2

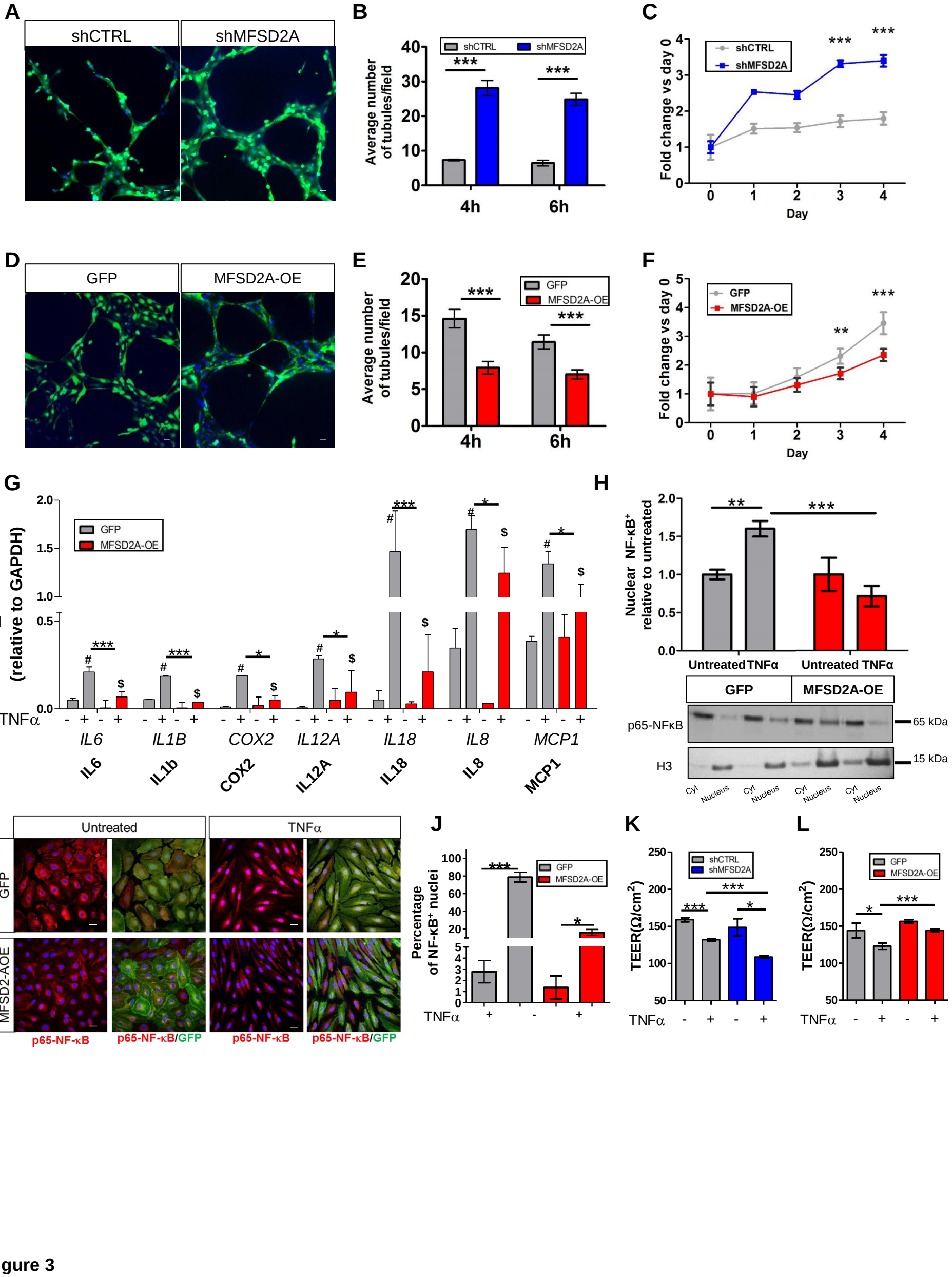
A
shCTRL
shMFSD2A
B
shCTRL
shMFSD2A
Average number of tubules/field
4h
6h
C
shCTRL
shMFSD2A
Fold change vs day 0
Day
D
GFP
MFSD2A-OE
E
GFP
MFSD2A-OE
Average number of tubules/field
4h
6h
F
GFP
MFSD2A-OE
Fold change vs day 0
Day
G
GFP
MFSD2A-OE
2-ΔCt (relative to GAPDH)
TNFα
IL6
IL1B
COX2
IL12A
IL18
IL8
MCP1
H
Nuclear NF-κB+ relative to untreated
Untreated
TNFα
GFP
MFSD2A-OE
p65-NFκB
H3
65 kDa
15 kDa
Cyt
Nucleus
I
Untreated
TNFα
GFP
MFSD2-AOE
p65-NF-κB
p65-NF-κB/GFP
J
Percentage of NF-κB+ nuclei
GFP
MFSD2A-OE
TNFα
K
shCTRL
shMFSD2A
TEER(Ω/cm2)
TNFα
L
GFP
MFSD2A-OE
TEER(Ω/cm2)
TNFα

Figure 3

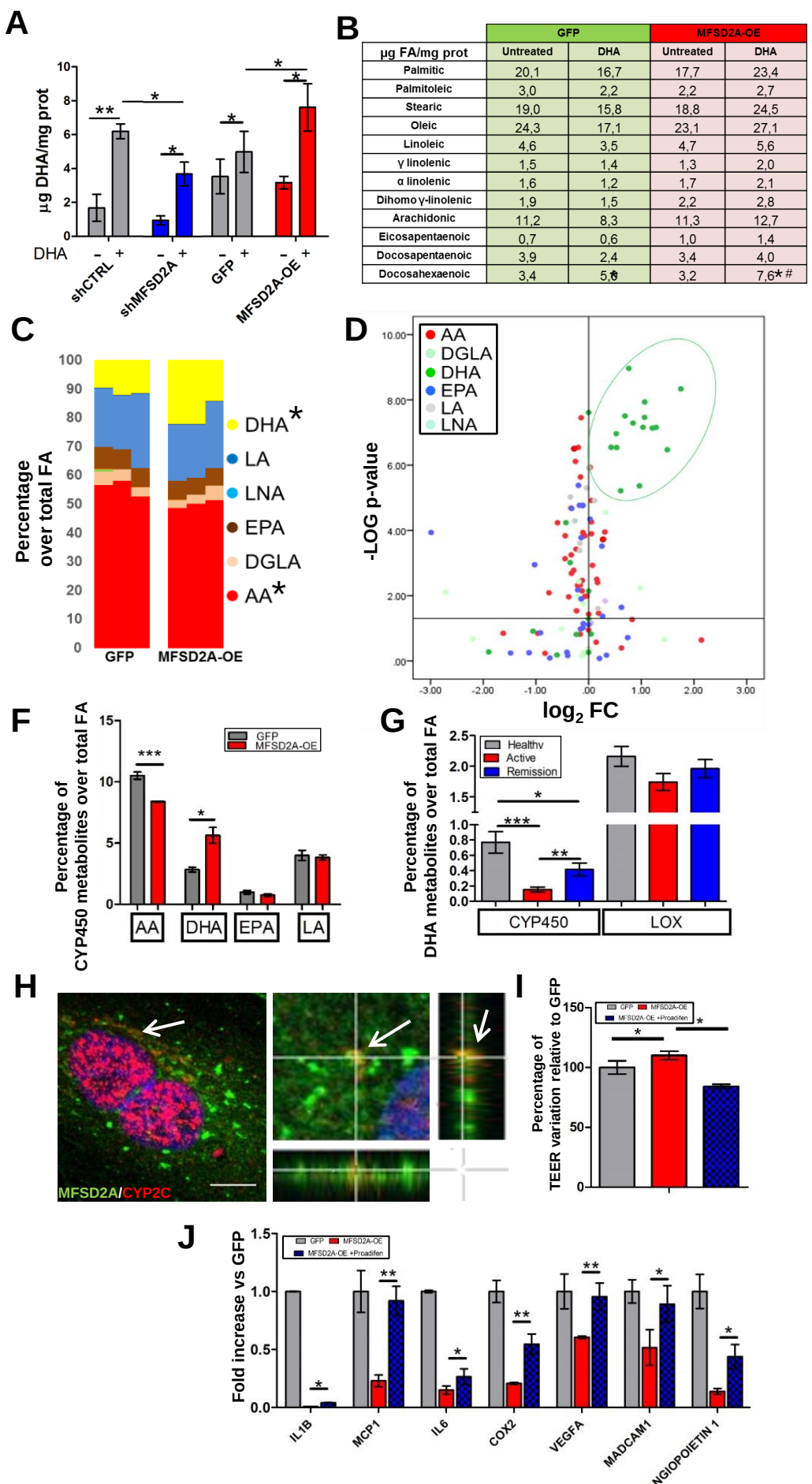

µg FA/mg prot	GFP		MFSD2A-OE	
	Untreated	DHA	Untreated	DHA
Palmitic	20,1	16,7	17,7	23,4
Palmitoleic	3,0	2,2	2,2	2,7
Stearic	19,0	15,8	18,8	24,5
Oleic	24,3	17,1	23,1	27,1
Linoleic	4,6	3,5	4,7	5,6
γ linolenic	1,5	1,4	1,3	2,0
α linolenic	1,6	1,2	1,7	2,1
Dihomo γ-linolenic	1,9	1,5	2,2	2,8
Arachidonic	11,2	8,3	11,3	12,7
Eicosapentaenoic	0,7	0,6	1,0	1,4
Docosapentaenoic	3,9	2,4	3,4	4,0
Docosahexaenoic	3,4	5,6	3,2	7,6* #

Figure 4

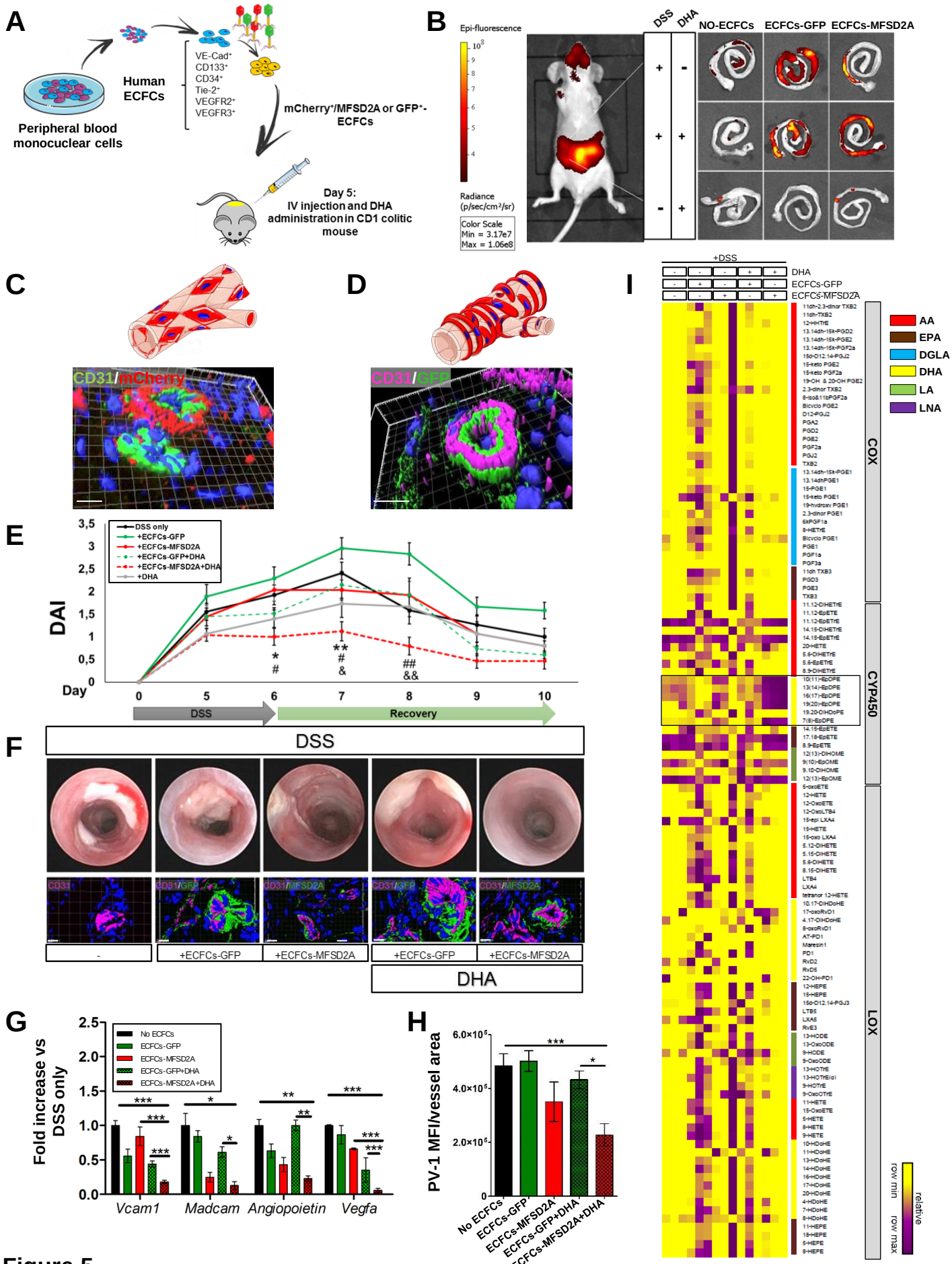
A
Human ECFCs
Peripheral blood monocuclear cells
VE-Cad+
CD133+
CD34+
Tie-2+
VEGFR2+
VEGFR3+
mCherry+/MFSD2A or GFP+-ECFCs
Day 5:
IV injection and DHA administration in CD1 colitic mouse
B
Epi-fluorescence
Radiance (p/sec/cm²/sr)
Color Scale
Min = 3.17e7
Max = 1.06e8
DSS
DHA
NO-ECFCs
ECFCs-GFP
ECFCs-MFSD2A
C
CD31/mCherry
D
CD31/GFP
E
DSS only
+ECFCs-GFP
+ECFCs-MFSD2A
+ECFCs-GFP+DHA
+ECFCs-MFSD2A+DHA
+DHA
DAI
Day
DSS
Recovery
F
DSS
CD31
CD31/GFP
CD31/MFSD2A
-
+ECFCs-GFP
+ECFCs-MFSD2A
+ECFCs-GFP
+ECFCs-MFSD2A
DHA
G
No ECFCs
ECFCs-GFP
ECFCs-MFSD2A
ECFCs-GFP+DHA
ECFCs-MFSD2A+DHA
Fold increase vs DSS only
Vcam1
Madcam
Angiopoietin
Vegfa
H
PV-1 MFI/vessel area
No ECFCs
ECFCs-GFP
ECFCs-MFSD2A
ECFCs-GFP+DHA
ECFCs-MFSD2A+DHA
I
+DSS
DHA
ECFCs-GFP
ECFCs-MFSD2A
AA
EPA
DGLA
DHA
LA
LNA
COX
CYP450
LOX
row min
row max
relative

Figure 5

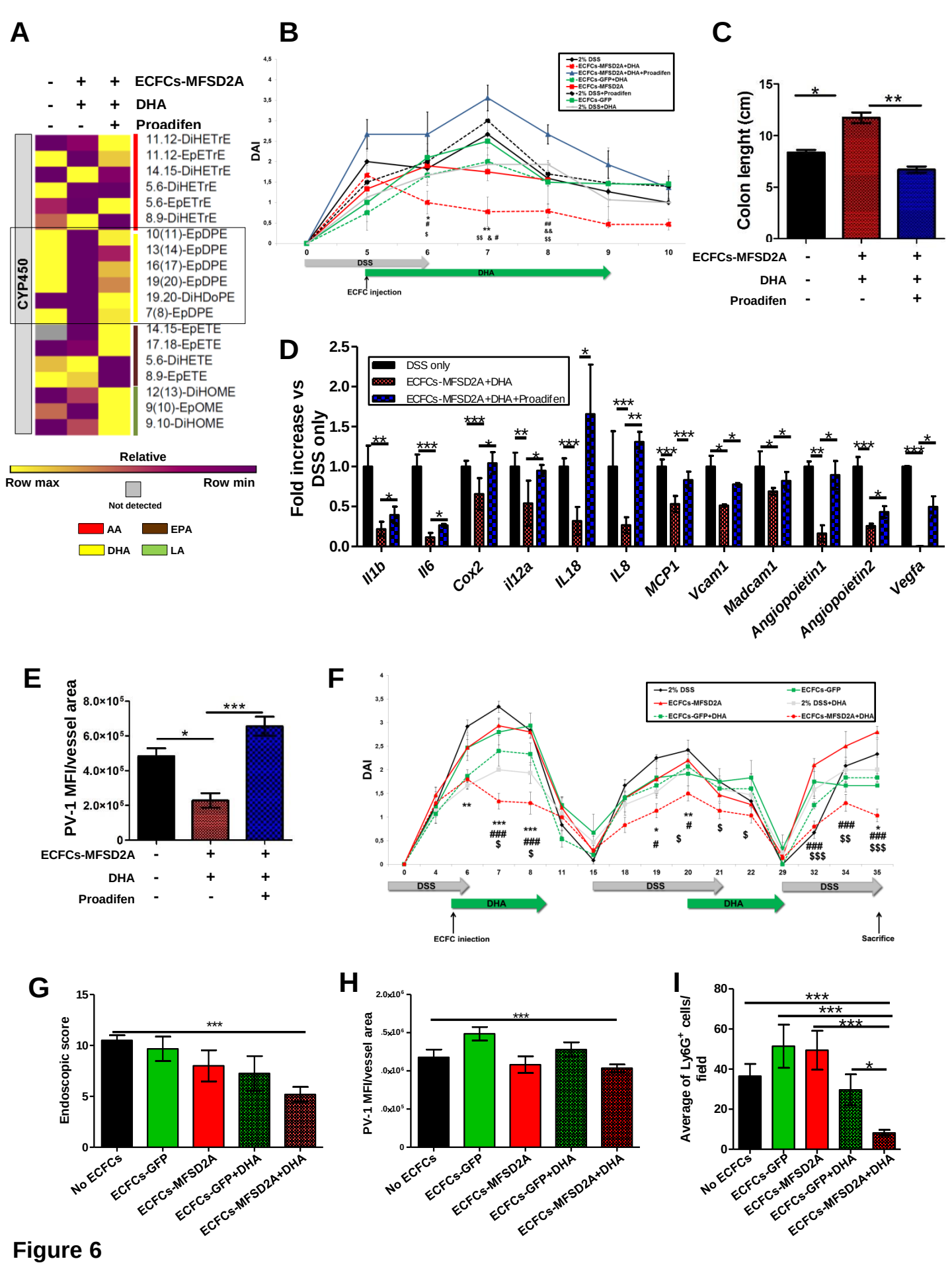
A
ECFCs-MFSD2A
DHA
Proadifen
11.12-DiHETrE
11.12-EpETrE
14.15-DiHETrE
5.6-DiHETrE
5.6-EpETrE
8.9-DiHETrE
10(11)-EpDPE
13(14)-EpDPE
16(17)-EpDPE
19(20)-EpDPE
19.20-DiHDoPE
7(8)-EpDPE
14.15-EpETE
17.18-EpETE
5.6-DiHETE
8.9-EpETE
12(13)-DiHOME
9(10)-EpOME
9.10-DiHOME
CYP450
Relative
Row max
Row min
Not detected
AA
EPA
DHA
LA
B
DAI
2% DSS
ECFCs-MFSD2A+DHA
ECFCs-MFSD2A+DHA+Proadifen
ECFCs-GFP+DHA
ECFCs-MFSD2A
2% DSS+Proadifen
ECFCs-GFP
2% DSS+DHA
DSS
DHA
ECFC injection
C
Colon lenght (cm)
ECFCs-MFSD2A
DHA
Proadifen
D
Fold increase vs DSS only
DSS only
ECFCs-MFSD2A+DHA
ECFCs-MFSD2A+DHA+Proadifen
Il1b
Il6
Cox2
il12a
IL18
IL8
MCP1
Vcam1
Madcam1
Angiopoietin1
Angiopoietin2
Vegfa
E
PV-1 MFI/vessel area
ECFCs-MFSD2A
DHA
Proadifen
F
DAI
2% DSS
ECFCs-GFP
ECFCs-MFSD2A
2% DSS+DHA
ECFCs-GFP+DHA
ECFCs-MFSD2A+DHA
DSS
DHA
ECFC iniection
Sacrifice
G
Endoscopic score
No ECFCs
ECFCs-GFP
ECFCs-MFSD2A
ECFCs-GFP+DHA
ECFCs-MFSD2A+DHA
H
PV-1 MFI/vessel area
I
Average of Ly6G+ cells/ field

Figure 6

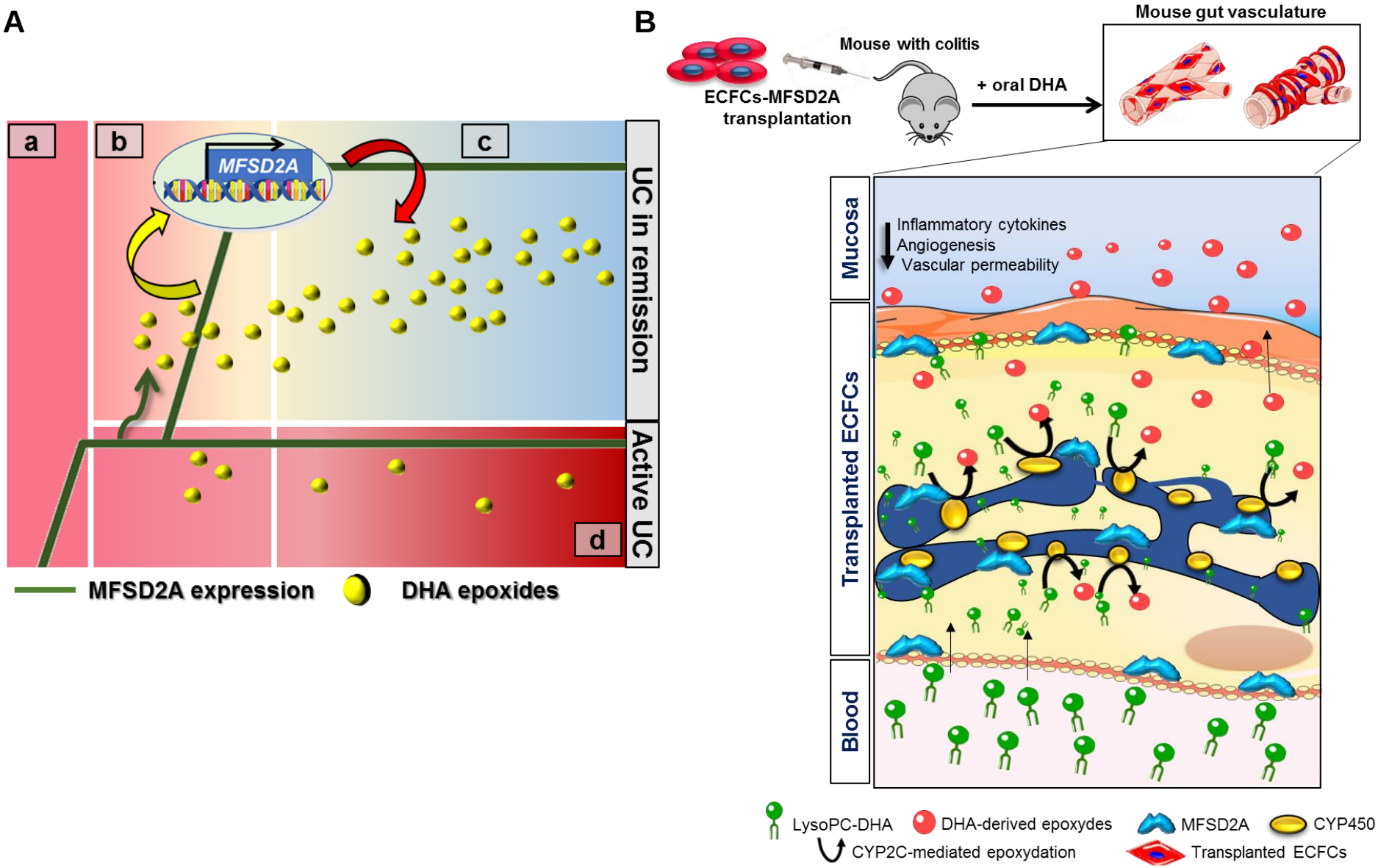
A
a
b
c
d
MFSD2A
UC in remission
Active UC
MFSD2A expression
DHA epoxides
B
Mouse with colitis
ECFCs-MFSD2A
transplantation
+ oral DHA
Mouse gut vasculature
Mucosa
Transplanted ECFCs
Blood
Inflammatory cytokines
Angiogenesis
Vascular permeability
LysoPC-DHA
DHA-derived epoxydes
MFSD2A
CYP450
CYP2C-mediated epoxydation
Transplanted ECFCs

Figure 7

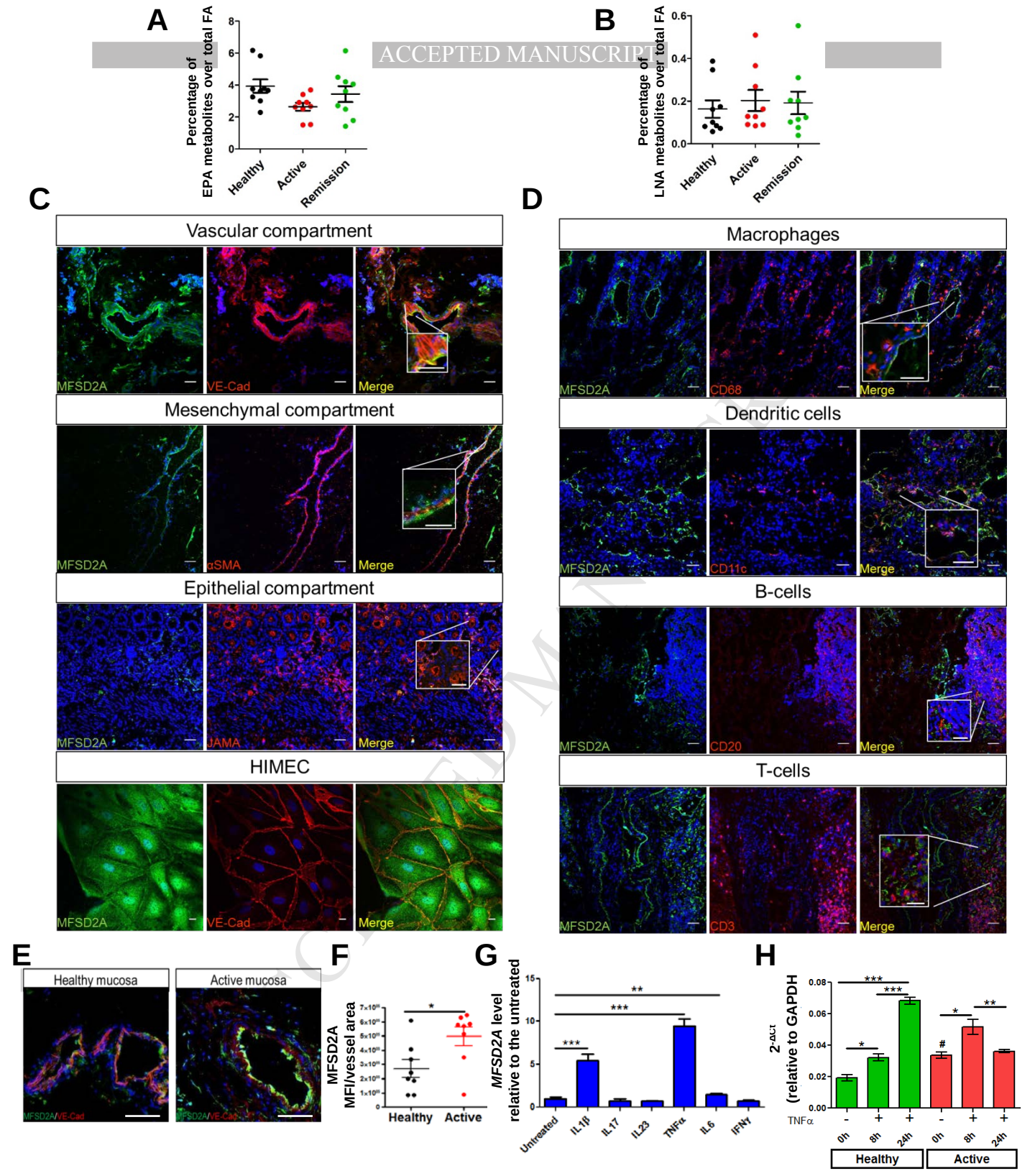

Supplementary Figure 1. MFSD2A is modulated under inflammatory conditions. Related to Figure 1 and 2.
(*A and B*) Percentage variations of EPA- (*A*) and LNA- (*B*) derived lipid mediators over total LC-MS/MS-detected fatty acids (FA) (n=9 per group). (*C* and *D*) Representative immunofluorescence images of cross-sections from human healthy colons stained for MFSD2A, VE-Cadherin (VE-Cad), α-Smooth Muscle Actin (αSMA), Junction adhesion molecule (JAM-A) (*C*), and CD68, CD11c, CD20, CD3 and DAPI (blue) (*D*). n=5 images per colon for 8 patients. (*E* and *F*) Representative confocal images of human colonic mucosa from healthy and patients with active UC, stained for MFSD2A, VE-Cadherin (VE-Cad), and DAPI (blue) (*E*) and relative quantification (*F*) of MFSD2A mean fluorescence intensity (MFI)/per vessel area (μm^2). n=5 images for n=8 patients per group. (*G*) *MFSD2A* transcript fold change relative to untreated upon indicated inflammatory cytokine stimulation n=3 per group. (H) *MFSD2A* transcript levels of healthy and UC-HIMECs relative to GAPDH, upon TNFα stimulation at 0, 8 and 24 hours. n=3 per group; # refers to untreated active vs untreated healthy.
*P and #P < 0,05; **P <0,01; ***P<0,005. All data are represented as mean ±s.e.m. Scale bars 50 µm.

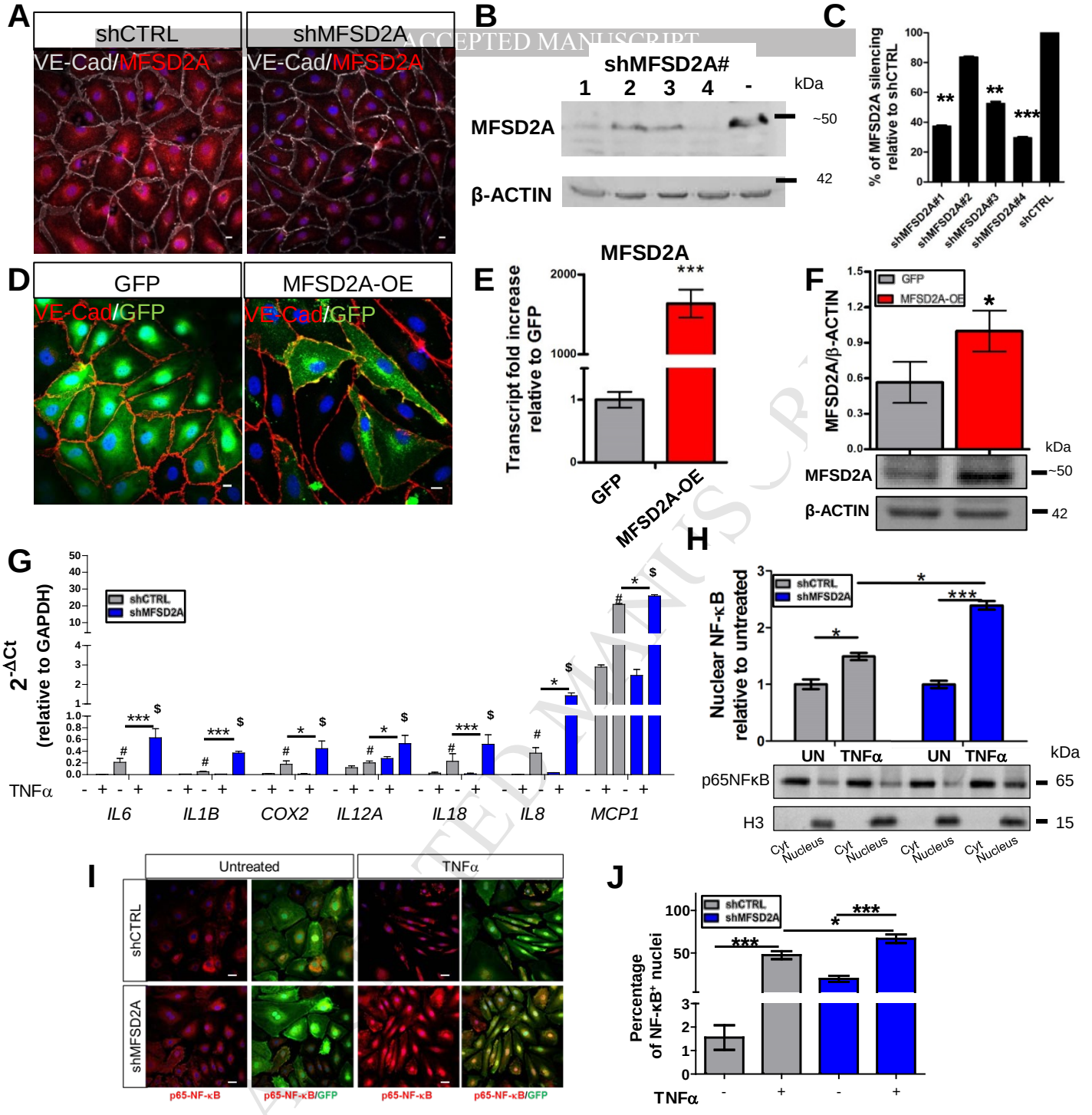

Supplementary Figure 2. MFSD2A modulates TNFα-induced response of HIMECs. Related to Figure 3.

(*A*) Representative confocal images of shMFSD2A and shCTRL HIMECs stained for MFSD2A, VE-Cadherin (VE-Cad, and DAPI (blue). (*B and C*) Western blot analysis performed on HIMECs transduced with 4 different shRNAs against *MFSD2A.* Representative bands (B) and quantification of *MFSD2A* silencing (C) in shMFSD2A versus shCTRL cells. shRNA #4 was used for all the subsequent experiments (n=4 lines of HIMECs). (D) Representative confocal images of MFSD2A-OE and control GFP HIMECs stained for MFSD2A, VE-Cadherin (VE-Cad), and DAPI (blue). (E) Quantification of *MFSD2A* expression in MFSD2A-OE and GFP HIMECs by qRT-PCR (n=3 group). (*F, top*) Western blot analysis of MFSD2A expression in protein extracts of MFSD2A-OE and GFP HIMECs. β-actin was used as loading control (n=3 group). (*F, bottom*) Representative bands. (*G*) Expression profile of inflammatory markers in untreated and TNFα-stimulated shMFSD2A and relative control HIMECs by qRT-PCR (n=3 replicates per condition of 5 independent experiments; # refers to untreated shCTRL vs TNFα-treated shCTRL; $ refers to untreated shMFSD2A vs TNFα-treated shMFSD2A; *refers to TNFα-treated shCTRL vs TNFα-treated shMFSD2A). (*H*) Western blot analysis (top) and representative bands (bottom) of the NF-κB-p65 subunit in nuclear and cytosolic protein extracts of unstimulated (UN) and TNFα-stimulated shMFSD2A and shCTRL HIMECs. Histone H3 (H3) was used as loading control (n=3 replicates per condition of 3 independent experiments). (*I and J*) Representative immunofluorescence (I) of untreated and TNFα-stimulated shMFSD2A and shCTRL HIMECs stained for NF-κB p65 subunit, GFP, and DAPI (blue) and relative quantification (J). Data are expressed as percentage of NFκB p65^{+} nuclei over the total nuclei (n= 3 replicates per condition of 3 independent experiments).

$^{*}P < 0,05$; $^{**}P< 0,1$; $^{***}P < 0,005$; $^{\#}P < 0,005$, $^{\$}P < 0,005$. All data are represented as mean ±s.e.m. Scale bars, 10 μm.

A

µg FA/mg prot	shCTRL		shMFD2A	
	Untreated	DHA	Untreated	DHA
Palmitic	5,8	4,5	6,4	10,0
Palmitoleic	0,6	0,3	1,1	1,3
Stearic	6,8	7,0	4,2	6,5
Oleic	12,3	10,7	7,5	11,4
Linoleic	1,3	1,3	1,1	1,7
γ linolenic	0,1	0,2	0,2	0,3
α linolenic	0,9	0,9	0,6	0,8
Dihomo γ-linolenic	0,7	0,7	0,4	0,6
Arachidonic	4,7	4,7	3,2	4,8
Eicosapentaenoic	0,2	0,2	0,1	0,2
Docosapentaenoic	1,4	1,6	0,9	1,1
Docosahexaenoic	1,7	6,1	0,9	3,6

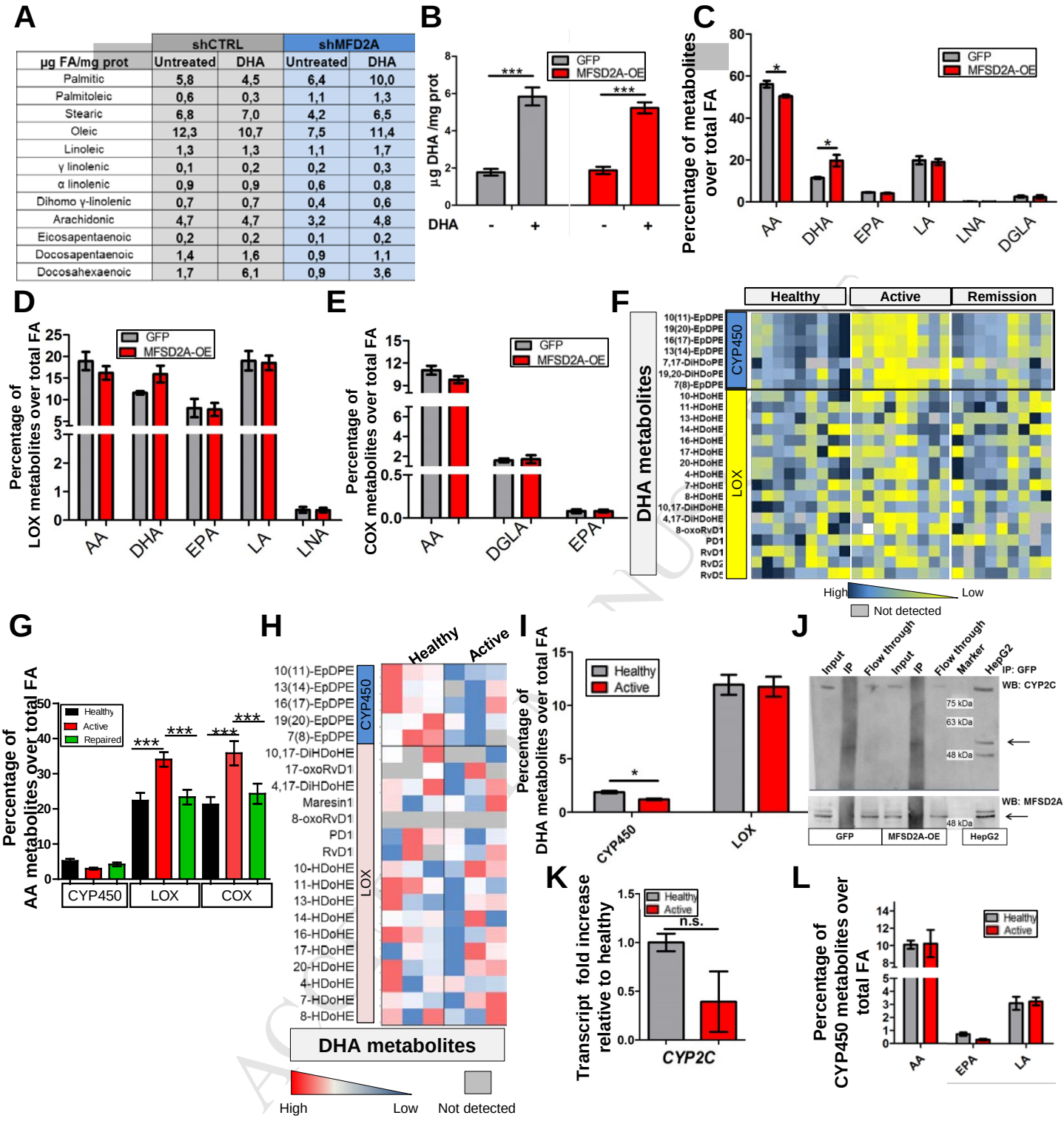

Supplementary Figure 3. MFSD2A modulates epoxygenation of DHA in HIMECs. Related to Figure 4.

(*A*) Table listing µg of fatty acids/mg protein detected by Gas-Chromatography on shMFSD2A and shCTRL control HIMECs with or without DHA treatment (n= 5 per group; * refers to +DHA vs untreated; # refers to +DHA-shMFSD2A vs +DHA-shCTRL). (*B*) DHA/mg protein in healthy and active UC-HIMECs with or without DHA treatment (n=5 per group) . (*C-E*) Percentage of AA-, DHA-, EPA-, LA-, LNA-, DGLA- (C), LOX- (D), and COX- (E) derived metabolites over the total fatty acids (FA) analyzed by LC-MS/MS in MFSD2A-OE and GFP HIMECs (n=3 per group). (*F*) Heat map showing significant variations of DHA metabolites classified on the basis of CYP450, and LOX enzymatic pathways in the mucosa of healthy patients, patients with UC and patients undergoing remission (n=9 per group). (*G*) Percentage of CYP450-, LOX- and COX-derived AA metabolites over total fatty acids (FA) detected by LC-MS/MS in endoscopic mucosal biopsies of healthy patients, patients with UC and patients undergoing remission (n=9 per group). (*H*) Heat map showing significant variations of DHA metabolites classified on the basis of CYP450, and LOX enzymatic pathways in healthy and active UC-HIMECs (n=3 per group). (*I*) Percentage of CYP450- and LOX-derived DHA metabolites over total fatty acids (FA) detected by LC-MS/MS in healthy and active UC-HIMECs (n=3 per group). (*J*) Co-IP assay by using an anti-GFP antibody of MFSD2A-OE and GFP HIMECs. HepG2 cell line was used as positive control for CYP2C (n=2 independent experiments). (*K*) *CYP2C* transcript levels quantified by qRT-PCR in healthy and active UC-HIMECs (n=5 per group). (*L*) Percentage of CYP450-derived metabolites in healthy and active UC-HIMECs (n=3 per group).

*P < 0,05; **P < 0,01; ***P<0,005; #P < 0,05. All data are represented as mean ±s.e.m.

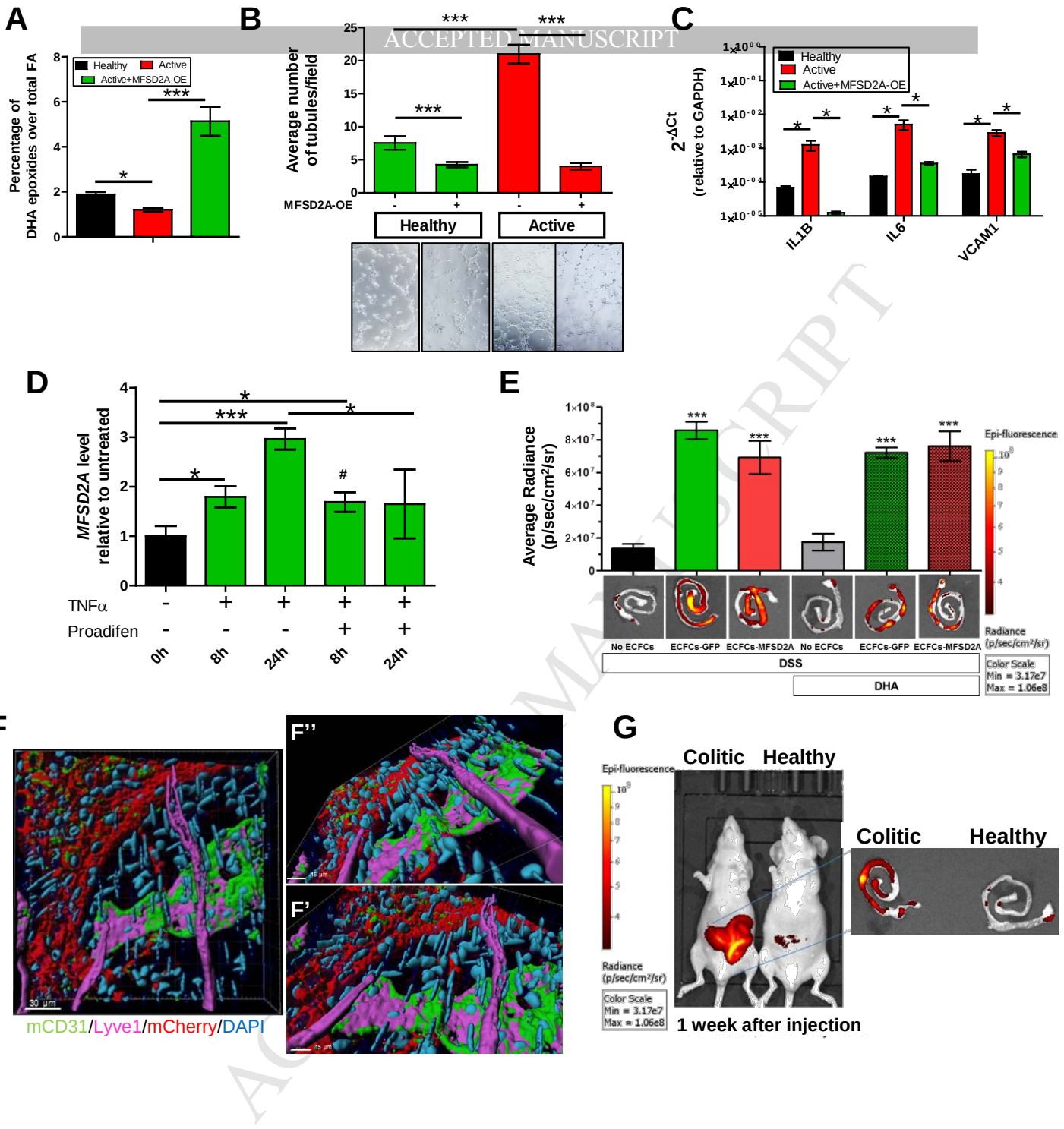

Supplementary Figure 4. MFSD2A overexpression corrects UC-HIMECs phenotype. Related to Figure 4 and 5.
(*A*) Percentage of CYP450-derived DHA epoxides over total fatty acids (FA) in healthy, UC and MFSD2A-OE UC-HIMECs (n=3 per group). (*B*) Tubule quantification (top) of phase contrast images (bottom) of healthy and UC-HIMECs at 4 hours after plating (n=3 replicates per n=5 patients/time point). (*C*) inflammatory marker transcript levels of healthy, UC active and active MFSD2A-OE UC-HIMECs relative to GAPDH (n=5 per group). (*D*) *MFSD2A* transcript of healthy HIMECs relative to GAPDH, upon TNFα stimulation and Proadifen treatement at the indicated time points (n=3 replicates of 2 independent experiments; # refers to 8h-TNFα-treated +Proadifen vs untreated HIMECs). (*E*) Radiance quantification of IVIS live images of colons isolated from colitic mice one week after ECFCs injection, at the indicated conditions (n=5 mice for 2 independent experiments). (*F*) Tridimensional reconstruction of confocal images performed on whole mount staining of colons isolated from ECFCs-GFP/mCherry-transplanted colitic mice one week after injection, with 2 different z projections (*F' and F''*). Tissues were stained for murine CD31 (mCD31), Lyve1, mCherry and DAPI (n= 2 independent experiments with 3 mice per group). (*G*) Representative images of healthy and ECFCs-GFP/mCherry-transplanted colitic mice one week after injection, using IVIS *in vivo* imaging system to detect mCherry (n=5 mice for 2 independent experiments).
*P and #P < 0,05; ***P<0,005; #P < 0,05. All data are represented as mean ±s.e.m. Scale bars, 50 µm.

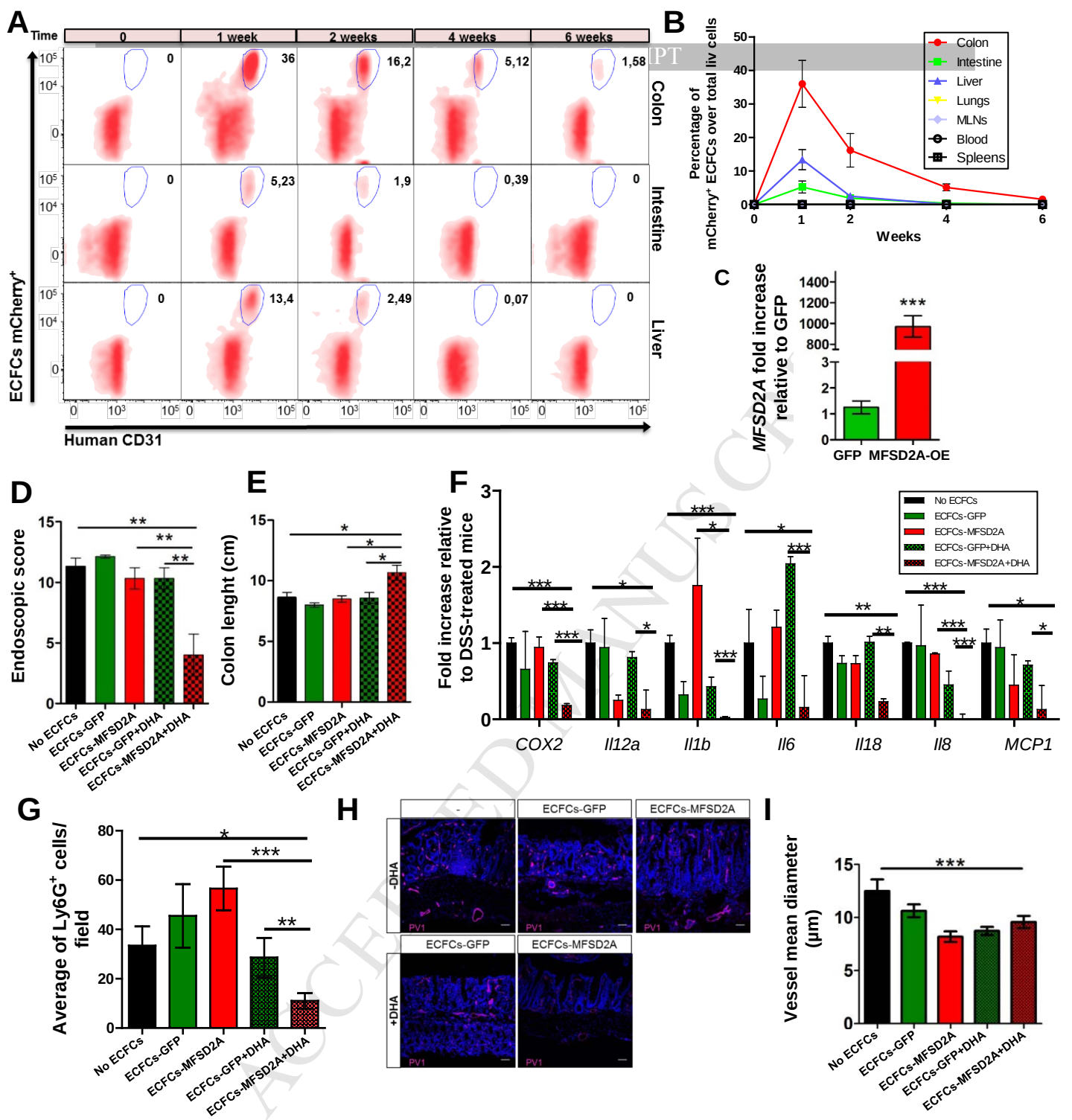

Supplementary Figure 5. ECFC integration into organs progressively decreases over time and ECFCs-MFSD2A-OE transplantation combined with DHA administration ameliorates intestinal inflammation in mice. Related to Figure 5.

(*A* and *B*) FACS analysis on colons, intestine, mesenteric lymphnodes (MLNs), liver, lungs, spleens and blood isolated from ECFC-mCherry-injected colitic mice at 0 (no ECFCs), 1, 2, 4 and 6 weeks after injection, stained for human CD31 and gated on live cells. Representative density plots (A) and relative quantification (B) of mCherry$^+$/hCD31$^+$ ECFCs over live cells in the indicated organs (n=4 mice for each time point). (*C*) MFSD2A transcript levels quantified in ECFCs-MFSD2A and ECFCs-GFP by qRT-PCR (n=3). (*D*) Endoscopic score of colons from ECFCs-MFSD2A in DHA-fed transplanted colitic mice 5 days after ECFC injection at the indicated conditions (n=5 mice per group of 2 independent experiments). (*E*) Colon length of ECFCs-MFSD2A-DHA-fed transplanted colitic mice at the indicated conditions 5 days after ECFC injection (n=5 mice per group of 2 independent experiments). (*F*) Inflammatory expression profile of colonic mucosa from ECFCs-MFSD2A-DHA-fed transplanted colitic mice at the indicated conditions 5 days after ECFC injection (n=5 mice per group of 2 independent experiments). (*G*) Quantification of Ly6G$^+$ cells (neutrophils) infiltration in colonic mucosa of DHA-fed colitic mice transplanted with ECFCs-MFSD2A at the indicated conditions (n=5 mice per group of 2 independent experiments). (*H*) Representative confocal images of mouse colons from ECFCs-MFSD2A-DHA-fed transplanted colitic mice at the indicated conditions stained for PV-1 and DAPI 5 days after ECFC injection (blue) (n=3 mice for 2 independent experiments). Scale bars, 50 µm. (*I*) Mean diameter quantification of colon vessels after whole mount staining of colitic mice at the indicated conditions 3 days after ECFC injection (n=5-8 mice per group of 2 independent experiments).

*P < 0,05 ; **P < 0,01 ; ***P < 0,005. All data are represented as ±s.e.m.

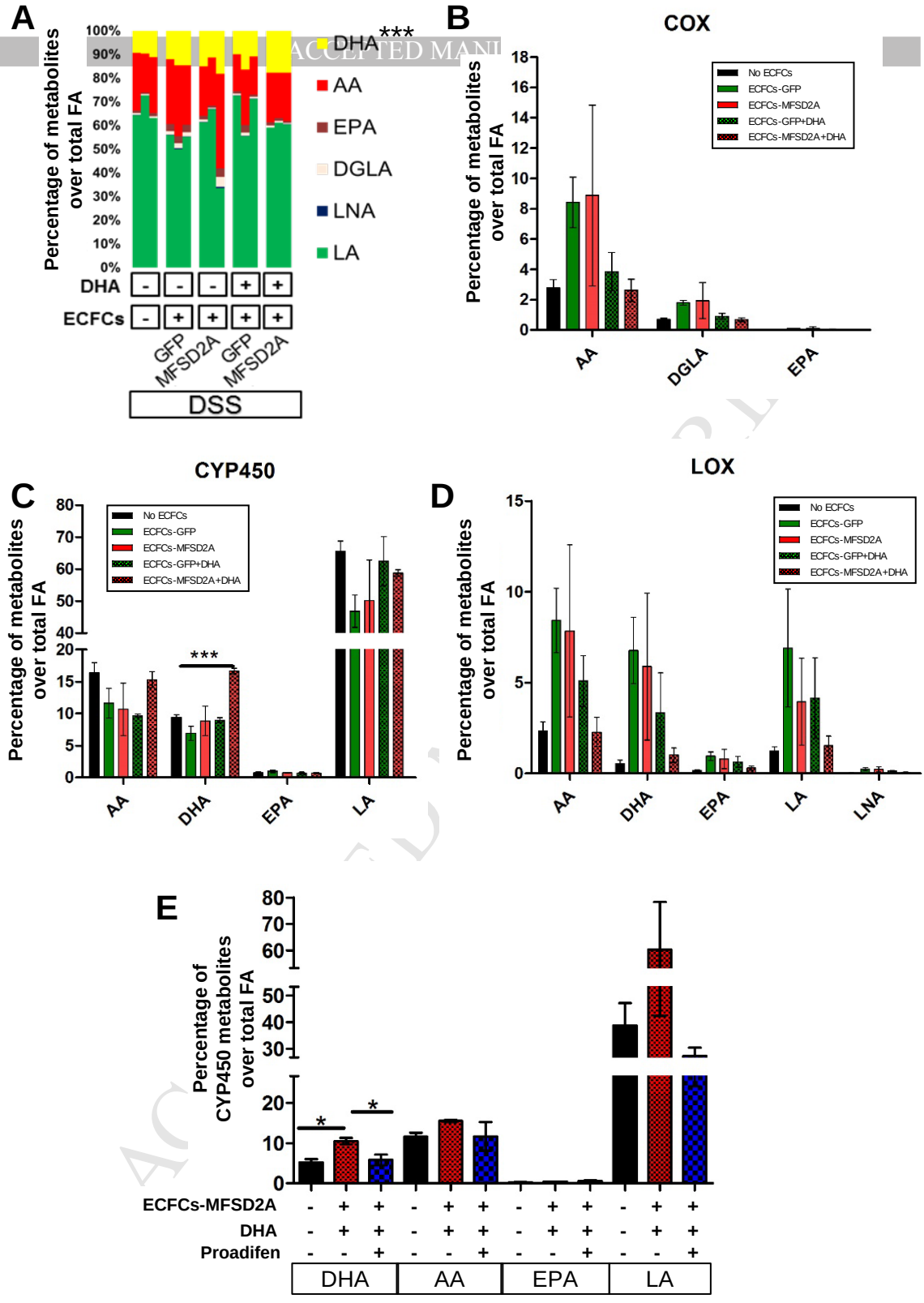

Supplementary Figure 6. Transplantation of ECFCs-MFSD2A-OE combined with DHA administration promotes CYP2C-dependent EpDPE production. Related to Figure 5 and 6

(*A*) Lipidomic analysis performed by LC-MS/MS on the colon extracts of DHA-fed colitic mice transplanted with ECFCs-MFSD2A at the indicated conditions, 3 days after ECFC injection. Data are expressed as percentage of the indicated PUFA-derived lipid mediators over total fatty acids (FA) (n=3 mice per group of 2 independent experiments). (*B-D*) Percentage variations of COX- (*B*), CYP450- (*C*) and LOX- (*D*) derived lipid mediators over total fatty acids (FA) in DHA-fed colitic mice transplanted with ECFCs-MFSD2A at the indicated conditions by LC-MS/MS analysis (n=3 mice per group of 2 independent experiments). (*E*) Percentage variations of CYP450-derived metabolites over total fatty acids (FA) in DHA-fed colitic mice transplanted with ECFCs-MFSD2A at the indicated conditions (n=3 mice per group of 2 independent experiments).

*P < 0,05; ***P < 0,005. All data are represented as ±s.e.m.

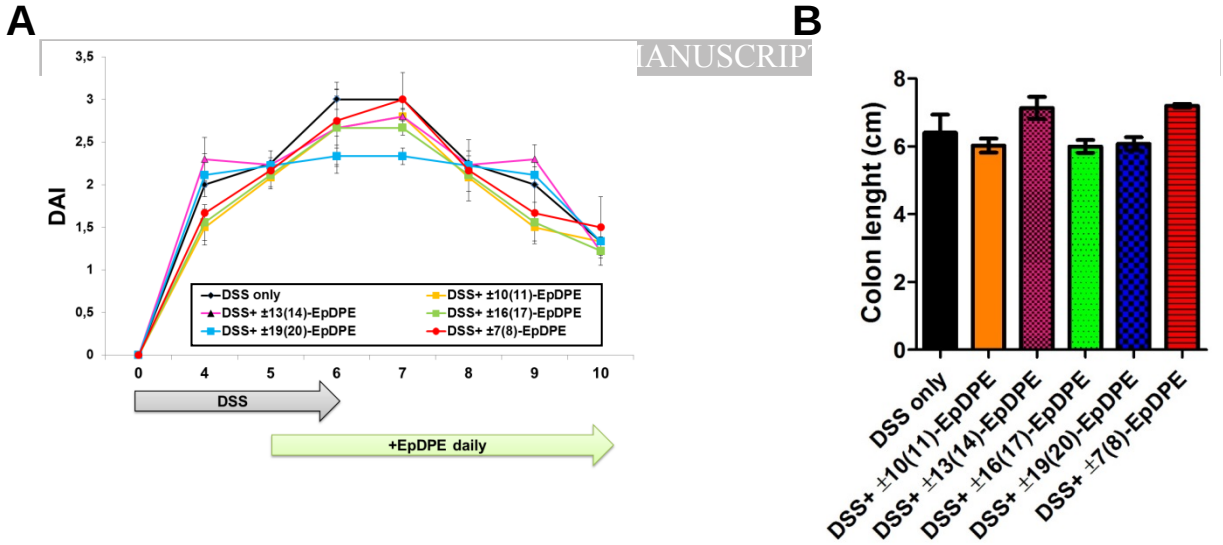

Supplementary Figure 7. Administration of single EpDPEs does not ameliorate intestinal inflammation. Related to Figure 6 (*A and B*) DAI (*A*) and colon length (*B*) of colitic mice intraperitoneally injected with racemic mixture of the indicated EpDPEs every day starting from day 5 after DSS treatmentt (n=of 5 mice per group for 3 independent experiments).
$^{*}P < 0,05$; $^{**}P < 0,01$; $^{***}P<0,005$. All data are represented as mean ±s.e.m.

Supplementary Tables

		Sex	Age	Endoscopic Mayo score	Riley index	Duration of disease (years)	Extent of colitis	Therapy in use	
Active		F	34	2	3	9	Descending colon, sigma, rectum	Steroids	Endoscopic biopsies
		F	56	2	3	N/A	Pancolitis	Mesalazine	
		M	33	3	4	9	Pancolitis	Anti-Jak	
		M	49	3	4	18	Descending colon, sigma, rectum	Mesalazine	
		M	40	2	3	5	Pancolitis	Mesalazine/Azathioprine	
		M	42	2	3	16	Descending colon, sigma, rectum	Mesalazine	
		F	68	2	3	12	Descending colon, sigma, rectum	Mesalazine	
		M	52	3	4	24	Descending colon, sigma, rectum	Mesalazine	
		M	57	3	4	12	Descending colon, sigma, rectum	Anti-JAK	
Remission		F	57	0	0	21	Descending colon, sigma, rectum	Mesalazine	
		M	20	0	0	1	Descending colon, sigma, rectum	anti-MAdCAM/Azathioprine	
		F	56	0	0	N/A	Pancolitis	Mesalazine	
		M	37	0	0	4	Pancolitis	Mesalazine; Infliximab	
		M	43	0	0	8	Pancolitis	Mesalazine	
		M	52	0	0	13	Descending colon, sigma, rectum	Infliximab	
		F	30	0	0	15	Descending colon, sigma, rectum	Mesalazine	
		F	70	0	0	26	Descending colon, sigma, rectum	Mesalazine/Azathioprine	
		M	48	0	0	N/A	Pancolitis	Mesalazine	
Healthy		M	56	/	/	/	Healthy	No treatment	
		M	55	/	/	/	Healthy	No treatment	
		M	39	/	/	/	Healthy	No treatment	
		M	77	/	/	/	Healthy	No treatment	
		F	59	/	/	/	Healthy	No treatment	
		M	79	/	/	/	Healthy	No treatment	
		M	56	/	/	/	Healthy	No treatment	
		M	42	/	/	/	Healthy	No treatment	
		F	45	/	/	/	Healthy	No treatment	

Supplementary Table 1. Characteristics of patients with active UC, UC in remission and healthy controls enrolled for endoscopic biopsy collection. Correlation between age/gender and disease status was not statistically significant (age-disease linear correlation: r^2=0,05421; F=1,433; p-value=0,2425; gender-disease linear correlation: r^2=0,001168; F= 0,02924; p-value=0,8656).

		Sex	Age	Duration of disease (years)	Extent of colitis	Therapy	Disease	
Active		M	46	18	Pancolitis	Steroids/Azathioprine/Mesalazin/Infliximab	UC	Surgical specimens
		M	43	20	Descending colon, sigma, rectum	Steroids/Azathioprine/Mesalazin/Infliximab	UC	
		M	51	9	Descending colon, sigma, rectum	Steroids/Azathioprine/Mesalazin/Infliximab	UC	
		F	68	9	Descending colon, sigma, rectum	Steroids/Azathioprine/Mesalazin/Infliximab	UC	
		M	57	7	Pancolitis	Steroids/Azathioprine/Mesalazin/Infliximab/Vedulizimab	UC	
		F	70	9	Descending colon, sigma, rectum	Steroids/Azathioprine/Mesalazina	UC	
		F	27	3	Descending colon, sigma, rectum	Steroids/Infliximab/Azathioprine	UC	
		F	24	4	Descending colon, sigma, rectum	Steroids/Mesalazina/Azathioprine	UC	
Healthy		M	79	/	/	No anti-inflammatory therapy	Colon cancer	
		F	73	/	/	No anti-inflammatory therapy	Colon cancer	
		F	38	/	/	No anti-inflammatory therapy	Colon cancer	
		M	71	/	/	No anti-inflammatory therapy	Colon cancer	
		F	73	/	/	No anti-inflammatory therapy	Colon cancer	
		M	58	/	/	No anti-inflammatory therapy	Colon cancer	
		M	56	/	/	No anti-inflammatory therapy	Diverticulosis	
		F	58	/	/	No anti-inflammatory therapy	Polyps	
		M	61	/	/	No anti-inflammatory therapy	Diverticulosis	

Supplementary Table 2. Characteristics of patients with active UC not responding to any treatment and control subjects enrolled for immunofluorescence analyses and HIMEC isolation from surgical biopsies. Correlation between age/gender and disease status was not statistically significant (age-disease linear correlation: r^2=0,2200; F=4,230; p-value=0,0575; gender-disease linear correlation: r^2=0,003086; F= 0,04644; p-value=0,8323).

		Forward 5'-3'	Reverse 5'-3'
Human	*IL1B*	AGGAGAATGACCTGAGCACC	AGCCTCGTTATCCCATGTGTC
	IL18	TTGCATCAACTTTGTGGCA	GCCAAAGTAATCTGATTCC
	IL12A	CCTTGCACTTCTGAAGAGATTGA	ACAGGGCCATCATAAAAGAGGT
	IL6	AACAAATTCGGTACATCCTCG	GCTTTCACACATGTTACTCTTG
	IL8	AACCCTCTGCACCCAGTTTTC	TTTTGCCAAGGAGTGCTAAAGA
	COX2	TGGAACGTTGTGAATAACATT	GTAAGTTGGTGGACTGTCAATC
	MCP1	AGTCTCTGCCGCCCTTCT	GTGACTGGGGCATTGATTG
	CYP2C	GAAAGAGCTAACAGAGGATTTG	AAAGTGGGATCACAGGGTGAGG
	MFSD2A	ACACGCCTTGTTTCCAGGAC	GCCAGCAGGTATGCCTTTTG
	MADCAM1	GGGGGCCGCACCTTCCAGCA	GTACAGGCCACCTCCGGGTCACC
	GAPDH	CATGAGAAGTATGACAACAGC	AGTCCTTCCACGATACCAAAG
Mouse	*Angiopoietin 1*	TCAGCCTTTGCACTAAAGAAGG	ACAGTCTCGAAATGGTTTCTCT
	Il18	AGCAGTCCCAACTAAGCAGTA	CAGCCAGTAGAGGATGCTGA
	Angiopoietin 2	GGAAACTGACTGATGTGGAAG	GAGTCTTGTCGTGTTTAG
	Madcam1	TTCACTGCCAGGTCACCATG	GTGAGGTCTGGCTCTGTAG
	Il8	TCGAGACCATTTACTGCAACAG	CATTGCCGGTGGAAATTCCTT
	COX2	*CACCCTGACATAGACAGTGAAAG*	*CTGGGTCACGTTGGATGAGG*
	Vcam1	TGGTGAAATGGAATCTGAACC	CCCAGATGGTGGTTTCCTT
	Nos2	GTTCTCAGCCCAACAATACAAG	GTGGACGGGTCGATGTCAC
	Vegfa	TTTACTGCTGTACCTCCACCA	ATCTCTCCTATGTGCTGGCTTT
	Il1b	AGTTGACGGACCCCAAAA	AGCTGGATGCTCTCATCAGG
	Il6	TAGTCCTCCCTACCCCAATTTC	TTGGTCCTTAGCCACTCCTTC
	Il12a	TCAGAATCACAACCATCAGCA	CGCCATTATGATTCAGAGACTG
	Gapdh	CGTGTTCCTACCCCCAATGT	TGTCATCATACTTGGCAGGTTTCT

Table S3. List of primers used for qRT-PCR

Supplemental Experimental Procedures

Patients

For endoscopic biopsies undergoing lipidomic, RNA and protein expression analyses, patients with UC undergoing endoscopy were diagnosed by physicians based on clinical, endoscopic and histological criteria. Endoscopic activities were assessed using the endoscopic Mayo score (normal: 0=inactive disease; erythema/decreased vascular pattern/mild friability/erosions: 1=mild disease; marked erythema/lack of vascular pattern/friability: 2=moderate disease; spontaneous bleeding/ulceration: 3=severe disease[1], and the Riley histological scoring system [2]. Active mucosal biopsies were defined by endoscopic Mayo score ≥2 and Riley Index≥3; biopsies under remission were defined by Mayo score=0 and Riley Index ≤1. Healthy endoscopic biopsies were obtained from patients undergoing routine check-up for non-IBD related diseases. Inclusion criteria were: 1) treatment with thiopurines (azathioprine± steroids), monoclonal antibodies and enzyme inhibitors (infliximab, vedolizumab, anti-MadCam, anti-JAK); 2) with a balanced mixed Western and Mediterranean diet; 2) with moderate or severe illness and decreased food intake. Exclusion criteria were: 1) age less than 16 or greater than 80 years; 2) patients taking trace elements (vitamins, fish oil), hypolipemiant drugs, or non-steroidal anti-inflammatory drugs in the previous 3 months; 3) patients with associated acute or chronic diseases other than IBD that could disturb fatty acid pattern; 4) patients with previous intestinal resection; 5) refusal to undergo endoscopic evaluation. All mucosal biopsy samples were snap-frozen and stored at –80℃ until use (see **Supplementary Table 1** for patient characteristics).
For HIMECs isolation and immunofluorescence analysis, intestinal tissues from involved areas were obtained from surgical specimens of patients with active UC not responding to any treatment. Healthy tissues from the large intestine of patients admitted for bowel resection due to colon cancer, polyps, or diverticulosis were used as controls (see **Supplementary Table 2** for patient characteristics). Inclusion and exclusion criteria were the same used for endoscopic biopsy selection.
Samples were not randomized and allocation and evaluation of clinical disease parameters were not blinded. The study was approved by the Humanitas Research Hospital ethics committee (Protocol number CE Humanitas ex D.M.8/2/2013-183/14). All subjects provided written informed consent.

Mice

CD1 nude mice (Charles River Laboratories) were maintained in our specific-pathogen free (SPF) animal facility and used at 8 weeks of age. All experiments were performed in accordance with the guidelines established in the Principle of Laboratory Animal Care (directive 86/609/EEC) and were approved by the Italian Ministry of Health. Housing was temperature controlled, with a 12-hour light/12-hour dark cycle. Procedures involving mice were conformed to institutional guidelines in agreement with national and international law and were approved by the ethics committee of the Humanitas Research Hospital. On the basis of our experience with animal models and according to animal-welfare policy (directive 86/609/EEC), which strongly suggests the use of a limited number of animals, we estimated that two experiments with n = 5 mice per group would allow us to reach statistical significance. Mice were not randomized and both experimental mice allocation and evaluation of clinical disease parameters were not blinded.

Liquid Chromatography tandem mass spectrometry (LC-MS/MS) analysis

Sample preparation. Endoscopic biopsies collected from the colonic mucosa of patients with active UC (n=9), UC in remission (n=9), and healthy subjects admitted for routine check-up not due to IBD-related symptoms (n=9), were snap frozen in dry ice. HIMECs were maintained in culture for 16 hours with phenol red-free DMEM and 0,4% BSA. Cells were then scraped, collected with the respective medium and snap-frozen in dry ice. For mouse colons, distal and proximal segments, were collected 3 days after ECFC injection and immediately snap frozen for lipid extraction.

LC-MS/MS and Lipidomic analysis. Tissue samples and cells were homogenized in phosphate buffer using a bead homogenizer (Precellys, Bertin Technologies), with a typical 1:9 ratio of solid sample to buffer. Samples (adjusted to a maximum volume of 1-2 ml) were spiked with a mixture of internal standards consisting of 15(S)-HETE-d_8, Leukotriene B_4-d_4, Resolvin D2-d_5, 14(15)-EpETrE-d_{11}, and prostaglandin E_1-d_4 (5 ng each) for recovery and quantitation, and mixed thoroughly. The samples were then extracted for PUFA metabolites using C18 extraction columns, as described earlier [3–6]. Briefly, the internal standard spiked samples were applied to conditioned C18 cartridges, washed with water followed by hexane and dried under vacuum. The cartridges were eluted with 0.5 ml methanol. The eluate was then dried under a gentle stream of nitrogen. The residue was re-dissolved in 50 µl methanol-25 mM aqueous ammonium acetate (1:1) and subjected to LC-MS analysis. HPLC was performed on a Prominence XR system (Shimadzu) using Luna C18 (3µ, 2.1x150 mm) column. The mobile phase consists of a gradient between A: methanol-water-acetonitrile

(10:85:5 v/v) and B: methanol-water-acetonitrile (90:5:5 v/v), both containing 0.1% ammonium acetate. The gradient program with respect to the composition of B is as follows: 0-1 min, 50%; 1-8 min, 50-80%; 8-15 min, 80-95%; and 15-17 min, 95%. The flow rate is 0.2 ml/min. The HPLC eluate was directly introduced to ESI source of QTRAP5500 mass analyzer (SCIEX) in the negative ion mode with following conditions: Curtain gas, GS1, and GS2: 35 psi, Temperature: 600 ˚C, Ion Spray Voltage: -2500 V, Collision gas: low, Declustering Potential: -60 V, and Entrance Potential: -7 V. The eluate was monitored by Multiple Reaction Monitoring (MRM) method to detect unique molecular ion – daughter ion combinations for each of the 125 transitions (to monitor a total of 156 lipid mediators). The MRM was scheduled to monitor each transition for 120 s around the established retention time for each lipid mediator. Optimized Collisional Energies (18 – 35 eV) and Collision Cell Exit Potentials (7 – 10 V) are used for each MRM transition. Mass spectra for each detected lipid mediator were recorded using the Enhanced Product Ion (EPI) feature to verify the identity of the detected peak in addition to MRM transition and retention time match with the standard. The data were collected using Analyst 1.6.2 software and the MRM transition chromatograms were quantitated by MultiQuant software (both from SCIEX). The internal standard signals in each chromatogram were used for normalization for recovery as well as relative quantitation of each analyte.

Isolation, culture and lentiviral transduction of HIMECs

HIMECs were isolated by enzymatic digestion of intestinal mucosal strips, followed by gentle compression to extrude endothelial cell clumps, which adhere to fibronectin-coated plates and were subsequently cultured in complete Endothelial Cell Growth Medium (EGM, Lonza). After 9 days in culture, cells were enzymatically digested (Trypsin, Life Technologies) and incubated with phycoerythrin-conjugated mouse anti-human CD31 antibody (BD Biosciences, clone WM59), as reported previously[7]. HIMECs were then sorted on a FACSAria IIU (BD Biosciences), using a FACSDiva software (version 6.1.3; BD Biosciences), by positive selection for CD31. Cultures of HIMECs were maintained at 37℃ in 5% CO_2, fed twice a week, and split at confluence. They were used between passages 2 and 6.
Treatments. HIMECs, grown at confluence, were treated with 20 ng/ml of recombinant human TNFα, or IL1-β, IL-17, IL-23, IL-6, and IFNγ (Peprotech, 300-01A) in EGM for 24 hours and then collected for RNA and protein extractions. To evaluate DHA retention by gas chromatography, HIMECs were treated with 10 µM DHA (Sigma Aldrich, D2534) in EGM for 16 hours. After incubation, cells were washed with fatty acid free 0,4%BSA (Sigma Aldrich, A7030) in PBS1x, detached with trypsin and collected for lipid quantification. For CYP2C inhibition experiments, HIMECs were treated with or without 30 µM SKF 525-A [8] (Proadifen, ENZO life science) in EGM for 24 hours in the presence of 20 ng/ml hTNFα.

Lentiviral transduction. Lentiviral particles production was performed by transient transfection of 293T cells according to standard protocols[9] and as previously described[10]. This cell line is competent to replicate vectors carrying the SV40 region of replication. It gives high titers when used to produce lentiviruses. It has been widely used for lentiviral production, gene expression and protein production.
Lentiviral vectors were purchased from OriGene (MFSD2A-GFP-tagged, pGFP-C-shLenti MFSD2A and scramble). The control plasmid for MFSD2A over-expressing vector, was obtained by excising the MFSD2A encoding sequence from the MFSD2A-GFP-tagged lentiviral plasmid and inserting the ATG codon upstream the GFP encoding sequence. For MFSD2A silencing, 4 different shRNAs were tested on HIMECs; the most efficient in knocking down MFSD2A expression was used for all experiments.
All cultures were Mycoplasma free.

Tubule Formation, Proliferation, and Endothelial Cell Permeability assays

HIMEC tube formation was assessed using Matrigel (BD Biosciences), as described previously [10,11]. Briefly, multi-well dishes were coated with 250 µL of complete medium containing 5 mg/mL Matrigel for 30 minutes at 37℃. MFSD2A silenced and MSFD2A-OE HIMECs were seeded in triplicate at a density of 5×10^4 in complete EGM. Cells were cultured on Matrigel for 4 and 6 hours, and inverted phase-contrast microscopy was used to assess and count endothelial tube-like structures. Five high-power fields per condition were examined at 10x magnification.
For proliferation assay, HIMECs were seeded in 96-well cell culture plates (1×10^3 cells/well) in EGM medium. At day 0, 1, 2, 3, and 4 cells were stained with 0.2% crystal violet (Sigma) dissolved in ethanol. Uptake of dye by cells on plates was eluted with 33% acetic acid in water. Plates were gently shaken for 20 min and the absorbance at 595 nm was measured by a Versamax microplate reader (Molecular Devices). The optical density of each sample was normalized to day 0 of each samples.
For cell permeability assay, MFSD2A silenced and MSFD2A-OE HIMECs were seeded on fibronectin-coated 0.4-µm pore-size Transwell Permeable Supports (Corning Costar, Cambridge, MA), cultured in complete culture medium and let to form a monolayer, as described previously [10]. After the establishment of a stable monolayer, HIMECs were stimulated for 24 hours with 20ng/ml TNFα (Peprotech, 300-01A) and/or with 30

µM Proadifen (Enzo Life Science) and assayed for permeability using a Millicall-ERS volt ohm meter (World Precision Instruments, New Haven, CT) to measure the transendothelial electrical resistance (TEER). The percentage of change in the transendothelial electrical resistance was calculated with respect to TNFα treated control cells (GFP or shCTRL).

Gas Chromatography (GC) fatty acid analysis

Cell lipid extraction. Lipids were extracted from $1x10^6$ cells with minor modification of Folch method [12]. Briefly, cells were homogenized with 500 µl of chloroform/methanol 1:2, centrifuged to recover the lipid extract and extracted again two times with chloroform/methanol 2:1, 1:1 (v/v). The total organic phase was dried under nitrogen and partitioned with 1 vol of water and 2 vol of chloroform/methanol/water 3/48/47 (v/v/v) to obtain an organic and an aqueous phase. The organic phase was dried and resuspended in chloroform/methanol 2:1, for further analysis. Each solvent used for extraction and analysis contained 0.045mM 3,5-Di-tert-4-butylhydroxytoluene (BHT) to avoid polyunsaturated fatty acids oxidation. Cell protein content was assessed according to Lowry et al. [13].

GC. The fatty acid composition of the organic phase was determined by gas chromatography as methylesters [12]. Lipids were derivatized with sodium methoxide in methanol 3.33% (w/v) to obtain fatty acid methyl esters (FAME). Prior to derivatization a known amount of internal standard (C17:0 triglyceride) was added to each sample to correct for yield and recovery of the reaction. FAME were rapidly extracted with hexane, dried and resuspended in a known volume of chloroform/methanol prior to injection into a gas chromatograph (Agilent Technologies 6850 series II, CA) equipped with flame ionization detector. The separation was achieved as follows: capillary column, AT Silar length 30 m, film thickness 0.25 µm; carrier gas, helium; injector temperature, 250°C; detector temperature, 275° C. The oven temperature was controlled at 50°C for 2 min and then increased at a rate of 10°C min-1 to 200° C, and maintained at t his temperature for 20 min. A standard mixture containing all fatty acid methylesters (Sigma Aldrich, MO) was injected as calibration for quantitative analysis. The amount of each fatty acid was normalized to protein content and expressed as µg/mg protein.

Immunofluorescence of HIMECs, human and murine colon tissues

HIMECs were fixed in 4% paraformaldehyde for 20 min at room temperature, washed in PBS1x and incubated for 1 hour at room temperature with the Blocking solution (10% goat or donkey serum, 0,1% Triton X-100 in PBS1x). HIMECs were then incubated overnight at 4°C with the following antibodies diluted in Blocking Solution: anti- VE-Cadherin (1:100, Santa Cruz, sc-6458), anti-MFSD2A (1:100, Abcam, ab105399), anti-GFP (1:500, Life Technologies, A11120), anti-p65 subunit of NF-κB (1:100, Santa Cruz, sc-372), anti-CALNEXIN (Blocking solution in 0,3% Triton X-100, 1:100, Santa Cruz, sc-23954), anti-CYP2C (1:200, ThermoFisher, PA5-36232).
Frozen sections (6 µm) of human and murine colon tissues were fixed in 4% paraformaldehyde solution for 10 min and then blocked and permeabilized with PBS containing 10% goat or donkey serum, and 0,1% Triton X-100 for 1 hr. After blocking, human colon sections were incubated overnight at 4°C with ant i-VE-Cadherin (1:100, Abcam, ab7047), anti-αSMA (1:500 , Sigma, a2547); anti-JAM-A (1:50, Thermo Fisher, 36-1700); anti-MFSD2A (1:100 LsBio, LS-B5348), anti-CD11c (1:500, BD Pharmingen, 550375), anti-CD68 (1:500, Dako, M 0876), anti-CD20 (1:200, Abcam, ab78237), anti-GFP (1:500, Life Technologies, A6455). Mouse colons collected 3 days after ECFC injection, were incubated overnight at 4°C with anti-CD31 (1: 100, LS-Bio, LS-B4737); anti-GFP (1:500, Life Technologies, A11120 and A6455), anti-mCherry (1:500, Abcam, Ab125096), anti-PV-1 (1:500, BD Pharmingen, 553849) or anti Ly6G (1:200, Abcam, ab25377).
All sections were then incubated for 1 hour at room temperature with secondary anti-rat, anti-mouse, anti-rabbit and anti-goat Alexa Fluor 488-conjugated; anti-rabbit, anti-mouse and anti-rat Alexa Fluor 594-conjugated; anti-goat, anti-mouse, anti-rat and anti-rabbit Alexa Fluor 647-conjugated antibodies (1:1000, Life Technologies), followed by incubation with DAPI for nuclear staining (1:25000, Invitrogen).
Samples were then washed with PBS1x, mounted with the Fluorescent Mounting Medium (Dako, S302380), and analyzed with a laser scanning confocal microscope (FluoView FV1000; Olympus).

Lys6G$^+$ cell quantification. Analysis of Ly6G$^+$ cells on mouse frozen colons were performed on fluorescent images acquired at a constant exposure time at ×40 magnification on a laser-scanning confocal microscope (FluoView FV1000, Olympus). Five fields for each colon were analyzed.

Immunofluorescence intensity measurements. Analysis of MFSD2A on human frozen colons and PV-1 on murine frozen sections were performed on fluorescent images acquired at a constant exposure time at ×20 magnification on a laser-scanning confocal microscope (FluoView FV1000, Olympus). Colons stained with secondary Abs alone were used to set the exposure time. Vascular structures with a lumen were analyzed

with ImageJ 1.45, and all images were within a linear intensity range of 0 to 6,231. To exclude nonspecific staining, structures less than 8 μm (1 μm = 6.8 pixels) in diameter were excluded. To calculate mean vessel intensity, the sums of pixel intensities per vessel were divided by the total vessel area (μm^2). The vessel mean fluorescence intensity (MFI) from 5 to 10 images per colon (*n* = 5 mice per experimental group) was averaged and compared between healthy and active human tissues for MFSD2A, and treated mice and control groups for PV-1.
Colocalization analysis between MFSD2A and CYP2C, and 3D image reconstruction of frozen sections were performed using Imaris Software.

Quantitative Real-Time Polymerase Chain Reaction (qRT-PCR).

RNA was extracted from cells, human and mouse colon tissues using the PureZOL RNA isolation reagent (Bio-Rad, Hercules, CA) according to manufacturer's instructions. RNA retrotranscription was performed with High Capacity cDNA Reverse Transcription Kits (Applied Biosystems, Carlsbad, CA). Quantitative Real time PCR reaction was performed with SYBR® Green Real-Time PCR Master Mix (Thermo Fisher Scientific) according to the manufacturer's instructions. The primer pairs used are summarized in the table below. The reactions were performed and analysed on ViiA7 Real-Time PCR System (Applied Biosystems). GAPDH expression was used as housekeeping gene. Data were calculated using the $2^{\wedge-\Delta\Delta Ct}$ method. Primers used are summarized in the **Table S3**.

Western blotting and Co-Immunoprecipitation

Endoscopic biopsies. Mucosal colonic biopsies from healthy patients and patients with active UC and UC in remission recruited as described above, were mechanically homogenized in lysis buffer containing 50 mM Tris-HCl, pH 7.4, 1mM ethylenediaminetetraacetic acid, pH 8.0, 150 mM NaCl, 1% Triton X-100, supplemented with a cocktail of protease inhibitors (Sigma), for protein extraction. Insoluble material was removed by centrifugation for 30 min at 14,000 *rpm* at 4℃. The concentration of proteins in each lysate was measured using the Bio-Rad protein assay (Bio-Rad Laboratories). 50 μg of protein extracts were separated on a 10% polyacrylamide gel and electrotransferred to a nitrocellulose membrane (Bio-Rad Laboratories). Nonspecific binding was blocked with Tris-buffered saline containing 5% non-fat dried milk and 0.1% Tween 20, followed by overnight incubation at 4℃ with anti-human MFSD2A (1:1000, Abcam, ab105399), anti-human β-ACTIN (1:1000, Santa Cruz, sc-1615). Membranes were washed for 1 hour with Tris-buffered saline containing 0.1% Tween 20 and then incubated for 1 hour with the appropriate horseradish peroxidase-conjugated secondary antibody (1:3000; GE Healthcare). The membranes were then incubated with Immobilon Western Chemilum (Millipore) for 1 minute, after which bands were detected by Chemidoc (Bio-Rad Laboratories), using Quantity One software. MFSD2A quantification was done by ImageJ 1.45 software using the anti-βACTIN detected bands as- normalizer.

HIMECs. Control and genetically modified cells with the indicated treatments and at the indicated time points were lysed with extraction buffer containing 50 mM Tris-HCl, pH 7.4, 1mM ethylenediaminetetraacetic acid, pH 8.0, 150 mM NaCl, 1% Triton X-100, supplemented with a cocktail of protease inhibitors (Sigma). The protein concentration of lysates, and immunoblotting was performed as described above, using the following primary antibodies: anti-human MFSD2A (1:1000, Abcam, ab105399), and anti-human β-ACTIN (1:1000, Santa Cruz, sc-1615), as loading control.

Co-Immunoprecipitation. For co-immunoprecipitation of MFSD2A with CYP2C, GFP and GFP-tagged MFSD2A-OE cells were grown at confluence on 100 mm Petri dishes cells. $2{,}5x10^6$ cells per condition were detached, collected and resuspended in lysis buffer containing Tris–HCl 50 mM, pH 8.0, NaCl 150 mM, and 1% NP-40 supplemented with protease and phophatase inhibitors (cOmplete™, Sigma-Aldrich) for 20 minutes, and then centrifuged for 15 min at 18,000 *g* at 4℃. Cell extracts were then pre-cleared with lysis buffer-containing protein-G agarose beads for 1 hour at 4℃. Pre-cleared lysates (1 mg) were incubated with an antibody against GFP (1 μg/ml in lysis buffer; Life Technologies, A11120) overnight at 4℃. After washing with lysis buffer, the immunoprecipitates were resuspended in SDS-sample buffer and immunoblotted, as described above. Nitrocellulose membranes were incubated with anti-human MFSD2A (1:1000, Abcam, ab105399), and anti-human CYP2C (1:1000, ThermoFisher, PA5-36232). Protein extracts from Human liver carcinoma cells (HepG2) were used as positive control for CYP2C.

For nuclear protein extraction, 200.000 control and genetically modified HIMECs with the indicated treatments were washed with ice-cold PBS1x and incubated for 5 min in ice with 200 μl of L1 lysis buffer containing 50mM Tris-HCl pH 8, 2 mM EDTA pH8, 0,1% NP-40, and 10% Glycerol. After scraping and centrifugation for 3' at 2000 rpm at 4℃, supernatants, composed of cytoplasmic proteins, were collected. The pellet, containing the nuclear fraction, was resuspended in buffer C (500mM KCl, 10% Glycerol, 25mM

HEPES pH 7,8). Both protein fractions were analyzed by western blot, as described above. Membranes were incubated with anti-human NFkB p65 subunit (1:1000, Santa Cruz, sc-372) and anti-hystone H3, gently provided by Dr. Chiara Porta (Humanitas Research Institute, Milan, Italy). The nuclear fraction was normalized on anti-hystone H3 detected band.

Induction and evaluation of colonic inflammation

For the DSS-induced acute colitis model, 8-week-old female mice were subjected to 1 oral cycle of 2% DSS (molecular mass, 40 kDa; MP Biomedicals) in drinking water for 6 days followed by 4 days in regular water. In this model, the disease activity index (DAI), recorded daily starting from day 0 to day 10, is based on the evaluation of different parameters characterizing experimental colitis induction and progression. Body weight, presence of gross blood in the feces, and stool consistency were recorded at the indicated time points. According to the criteria proposed by Cooper et al.[14], the DAI was determined by scoring changes in: weight loss (0 = none, 1 = 1%–5%, 2 = 5%–10%, 3 = 10%–20%, 4 = >20%); stool consistency (0 = normal, 2 = loose, 4 = diarrhea); and rectal bleeding (0 = normal, 2 = occult bleeding, 4 = gross bleeding). A 5-point (0-4) DAI was thus obtained.

*Endoscopic damage assessment***.** For monitoring of colitis, a high resolution mouse video endoscopic system was developed and used as previously described[7].

Adoptive transfer of engineered ECFCs, mice treatments and *in vivo* imaging.

Endothelial cells forming colony (ECFCs) were isolated and characterized as previously described by Colombo et al.[15]. Peripheral blood mononuclear cells (PBMCs) were isolated by gradient centrifugation, resuspended in EGM-2 medium (Lonza), and seeded onto human fibronectin (Sigma Aldrich)-coated 24-well plates. Non-adherent cells and debris were aspirated after one day of culture; adherent cells were washed and cultured in EGM-2 medium. ECFC colonies, identified by visual inspection using an inverted microscope, were detached from the original tissue culture plates by trypsinization (Euroclone) and replated onto 6-well tissue culture plates previously coated with type-I collagen (Corning Inc). ECFCs were maintained in EGM-2 medium at 37℃ in 5% CO2, fed three times a week, and split at confluence. ECFC phenotype was confirmed by flow cytometry, by assessing the expression of the endothelial markers CD31, KDR and CD146, while lacking the hematopoietic markers CD45 and CD14.

ECFCs were then transduced with MFSD2A-GFP-tagged and GFP control scramble lentiviruses (OriGene). The GFP control plasmid for MFSD2A over-expressing vector, was obtained by excising the MFSD2A encoding sequence from the MFSD2A-GFP-tagged lentiviral plasmid and inserting the ATG codon upstream the GFP encoding sequence. Both ECFCs overexpressing MSFD2A (ECFCs-MFSD2A) and control ECFCs (ECFCs-GFP) were double infected with mCherry lentiviral particles to monitor ECFC homing into the inflamed mucosa by live imaging analysis. The mCherry lentiviral vector was kindly provided by Dr. Marco Erreni, Humanitas Clinical and Research Center, Milan, Italy.

For DSS-induced acute colitis, mice were administered with 2% DSS for 6 days. At day 5 of DSS administration, mice were injected in the tail vein with $5x10^5$ ECFCs-GFP or ECFCs-MFSD2A and at the same time were administered with 1mg/g/mouse DHA-ethyl-ester (Cayman chemical) by oral gavage every day until sacrifice. In parallel, at day 5 of DSS a group of DHA-fed ECFCs-MFSD2A injected mice was intraperitoneally treated with 30mg/kg of Proadifen[16], every day until sacrifice.

In another set of experiments the following metabolites were intravenously injected (0,05 mg/Kg)[17] every day until sacrifice, starting at day 5 of DSS administration: ±10(11)-EpDPE, ±13(14)-EpDPE, ±16(17)-EpDPE, ±19(20)-EpDPE, ±7(8)-EpDPE (Cayman Chemical).

Mice were sacrificed 3 and or 5 days after ECFCs injection and/or DHA and Proadifen administration, when differences among groups reached the highest statistical significance, upon endoscopic evaluation. Colons were immediately frozen in dry ice for RNA extractions, and LC-MS/MS analysis or embedded in Cryoblock Compound for immunofluorescence studies. For long-term studies, mice were sacrificed 4 and 6 weeks after ECFCs transplantation. Two independent experiments of DSS-induced chronic colitis were performed with mixed cages of mice all derived from the same SPF source and with 2 different lots of DSS. Mice were treated according to the following scheme: 6 days of DSS, 1 week of water and finally, 6 days of DSS, 1 week of water and finally DSS until sacrifice at day 35 for tissue analysis. At day 5 of the first abnd second cycle, mice were injected with ECFCs and/or administered with DHA-ethyl-ester.

In vivo imaging was performed to confirm ECFCs engraftment and homing to the inflamed mucosa, before and after the sacrifice on the whole mouse and isolated colons respectively, using a Caliper Xenogen IVIS Spectrum (Caliper Life Sciences, Hopkinton, MA). A light image was obtained for anatomical orientation and mCherry fluorescence was detected using standard parameters, which include 12.9-cm field of view to observe 3 mice simultaneously, excitation filter = 570 nm, emission filter = 620 nm, f-stop 1, pixel binning 8, and 0.5 seconds exposure time. Images were analyzed using Living Imaging software and the region of interest (ROI) function. For *in vivo* imaging quantification, the radiance (p/sec/cm^2/sr) of the ROI was

automatically calculated by the Caliper Xenogen IVIS Spectrum Software. Three ROIs for each colon where used for calculating the average of radiance.

FACS analysis of mCherry-ECFCs-injected colitic mice

Nude CD1 colitic mice were injected with $5x10^5$ mCherry transduced ECFCs at day 5 of 2% DSS treatment. Not-injected colitic mice were used as controls. Mice were sacrificed 1, 2 4 and 6 weeks after ECFC injection. Organs were isolated and processed for the FACS.

Lungs, livers and lymphnodes were disrupted through a 70 µm filter (BD Falcon) with a 1 ml syringe plunger and washed with 10 ml of RPMI medium supplemented with 10% foetal calf serum and 20 mM Hepes. Lungs and livers were then centrifuged at 800 rpm for 10 minutes to discard debris. Ammonium-Chloride-Potassium (ACK) lysis buffer was used directly on pellets to remove red blood cells. All samples were washed with RPMI medium and centrifuged. Samples were then suspended in PBS and counted.

Colon and small intestines were cleaned with HBSS solution containing antibiotics and Hepes, and cut in small pieces. The epithelial layer was removed by incubating the intestine fragments with HBSS and EDTA solution at 37℃ under gentle agitation. Intestine fragments deprived from epithelial cells were chopped and digested with HBSS containing 5% foetal calf serum, Hepes, CaCl2, dispase and collagenase (Roche) and DNase at 37℃ under agitation. Digested fragments were further disrupted through a 100 µm filter (BD Falcon) with a 1 ml syringe plunger and washed with 10 ml of RPMI medium supplemented with 10% foetal calf serum and 20 mM Hepes. Single cell suspension was further filtered over a 70 µm filter (BD Falcon).

Blood was collected from mouse cheeks and collected in EDTA tubes (Greiner Mini Collect). 100 µl of blood was briefly lysed with 500 µl of ACK lysis buffer and washed with 1ml RPMI medium supplemented with 10% foetal calf serum and 20 mM Hepes.

Cell suspension from all organs were stained with LIVE/DEAD® Cell Stain Kit (Life Technologies), washed in PBS and analyzed by FACS (BD FACSCanto™ II - BD Biosciences). Data analysis was performed by FlowJo v10 software.

Whole Mount Staining and morphometric analysis of colonic vessels

Three days after ECFC injection, mice were anesthetized with 100 mg/kg ketamine and 50 mg/kg xylazine, and 10 mL of 1% paraformaldehyde fixative solution was perfused into the heart. Colons were removed from untreated and injected mice with the indicated treatments, and immersed in 1% paraformaldehyde fixative solution, overnight at 4℃. Tissues were then washed and incubated with hamster anti-CD31 (1:500; Millipore, MAB1398Z), rabbit anti-Lyve1 (1:500, Abcam, ab14917), rat anti-mCherry (1:500, ThermoFisher Scientific, M11217) antibodies diluted in PBS containing 0.3% Triton X-100, 2% bovine serum albumin, 5% goat serum, 0.01% glycine, and 0.1% sodium azide, overnight at 4℃. Anti-hamster Alexa Fluor 488, anti-rabbit Alexa Fluor 647 (1:500; Molecular Probes) and anti-rat Alexa Fluor 594 (1:500; Molecular Probes) were used as secondary antibodies, and incubated overnight at 4℃. Samples were then mounted with Vectashield (Vector Laboratories, Burlingame, CA) and imaged with a laser scanning confocal microscope (Fluoview FV1000; Olympus). Fluorescent images were acquired at a constant exposure time at 20× or 60× magnification on a laser scanning confocal microscope (FluoView FV1000; Olympus). Morphometric analysis of colon whole mounts was performed by 3D visualization of both hematic and lymphatic vessels. Images were taken as a *z* series stack using a ×10 objective and analyzed by Imaris Bitplane software, thus allowing visualization of the vessels in the submucosal and serosal-muscular layers. For each colon analyzed (n = 5–8 mice for each experimental group), both hematic and lymphatic vessel size were measured in 10 randomly chosen regions covered by vessels (each 1.0 mm^2 in area) and were represented as the mean value of diameters (µm).

Statistics

The sample size was calculated on the basis of the effect size derived from preliminary data. Normal distribution and source of variation were calculated automatically for every statistical comparison. Mean comparisons were calculated accordingly. Statistical analyses were performed with either Microsoft Excel or IBM SPSS and Graph Pad 5-Prism statistical packages. Data were represented as means ±s.e.m. Mean comparisons between two experimental conditions were analyzed with 2-tailed unpaired Student's t test. For three or more conditions, One-way ANOVA with Bonferroni's correction was used. Two-way ANOVA with Bonferroni's correction was used for the statistical analysis of DAI (in DSS-induced colitis experiments). P-values lower than or equal to 0.05 were considered statistically significant. Heatmap of data distributions were displayed with GENE-E software from Broad Institute (https://software.broadinstitute.org/GENE-E/).

Supplemental References

1. Schroeder KW, Tremaine WJ, Ilstrup DM. Coated oral 5-aminosalicylic acid therapy for mildly to moderately active ulcerative colitis. A randomized study. N Engl J Med 1987;317:1625–9.

2. Riley S a, Mani V, Goodman MJ, et al. Microscopic activity in ulcerative colitis: what does it mean? Gut 1991;32:174–8.

3. Maddipati KR, Zhou S-L. Stability and analysis of eicosanoids and docosanoids in tissue culture media. Prostaglandins Other Lipid Mediat 2011;94:59–72.

4. Maddipati KR, Romero R, Chaiworapongsa T, et al. Eicosanomic profiling reveals dominance of the epoxygenase pathway in human amniotic fluid at term in spontaneous labor. FASEB J 2014;28:4835–46.

5. Maddipati KR, Romero R, Chaiworapongsa T, et al. Lipidomic analysis of patients with microbial invasion of the amniotic cavity reveals up-regulation of leukotriene B4. FASEB J 2016;30:3296–3307.

6. Maddipati KR, Romero R, Chaiworapongsa T, et al. Clinical chorioamnionitis at term: the amniotic fluid fatty acyl lipidome. J Lipid Res 2016;57:1906–1916.

7. D'Alessio S, Correale C, Tacconi C, et al. VEGF-C-dependent stimulation of lymphatic function ameliorates experimental inflammatory bowel disease. J Clin Invest 2014;124:3863–78.

8. Brandon EFA, Meijerman I, Klijn JS, et al. In-vitro cytotoxicity of ET-743 (Trabectedin, Yondelis), a marine anti-cancer drug, in the Hep G2 cell line: influence of cytochrome P450 and phase II inhibition, and cytochrome P450 induction. Anticancer Drugs 2005;16:935–43.

9. Dull T, Zufferey R, Kelly M, et al. A third-generation lentivirus vector with a conditional packaging system. J Virol 1998;72:8463–71.

10. Tacconi C, Correale C, Gandelli A, et al. Vascular endothelial growth factor C disrupts the endothelial lymphatic barrier to promote colorectal cancer invasion. Gastroenterology 2015;148:1438–1451.e8.

11. D'Alessio S, Correale C, Tacconi C, et al. VEGF-C-dependent stimulation of lymphatic function ameliorates experimental inflammatory bowel disease. J Clin Invest 2014;124:3863–3878.

12. Corsetto PA, Cremona A, Montorfano G, et al. Chemical-physical changes in cell membrane microdomains of breast cancer cells after omega-3 PUFA incorporation. Cell Biochem Biophys 2012;64:45–59.

13. LOWRY OH, ROSEBROUGH NJ, FARR AL, et al. Protein measurement with the Folin phenol reagent. J Biol Chem 1951;193:265–75.

14. Cooper HS, Murthy SN, Shah RS, et al. Clinicopathologic study of dextran sulfate sodium experimental murine colitis. Lab Invest 1993;69:238–49.

15. Colombo E, Calcaterra F, Cappelletti M, et al. Comparison of Fibronectin and Collagen in Supporting the Isolation and Expansion of Endothelial Progenitor Cells from Human Adult Peripheral Blood. PLoS One 2013;8.

16. Gilroy DW, Edin ML, Maeyer RPH De, et al. CYP450-derived oxylipins mediate inflammatory resolution. Proc Natl Acad Sci U S A 2016;113:E3240-9.

17. Zhang G, Panigrahy D, Mahakian LM, et al. Epoxy metabolites of docosahexaenoic acid (DHA) inhibit angiogenesis, tumor growth, and metastasis. Proc Natl Acad Sci U S A 2013;110:6530–5.